Collective cell migration relies on PPP1R15-mediated regulation of the endoplasmic reticulum stress response

Yujun Chen, Jocelyn A. McDonald

PII: S0960-9822(24)00156-8
DOI: doi:10.1016/j.cub.2024.02.014
Reference: CURBIO 20067

Published in: *Current Biology*

Received date: 22 May 2023
Revised date: 19 December 2023
Accepted date: 7 February 2024

Cite this article as: Chen Y, McDonald JA, Collective cell migration relies on PPP1R15-mediated regulation of the endoplasmic reticulum stress response, *Current Biology*, doi:10.1016/j.cub.2024.02.014

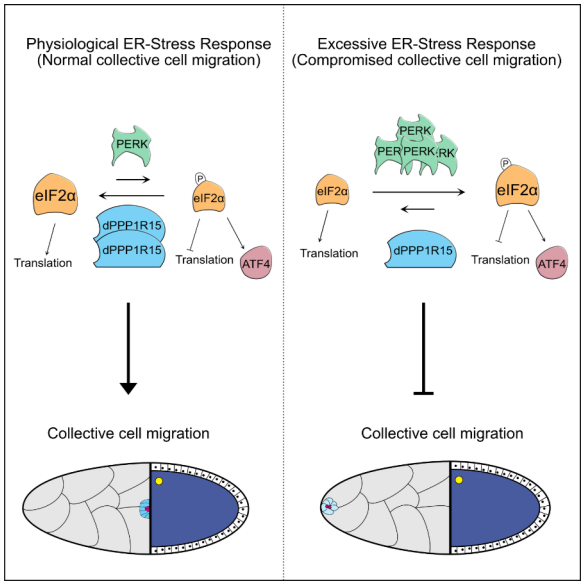

Collective cell migration relies on PPP1R15-mediated regulation of the endoplasmic reticulum stress response

Yujun Chen[1] and Jocelyn A. McDonald[1,2,3*]

[1]Division of Biology, Kansas State University, 1717 Claflin Road, Manhattan, KS 66506, USA

[2]Lead Contact

[3]Twitter: @JocMcDonald

[*]Correspondence: jmcdona@ksu.edu

Y.C. ORCID (0000-0003-3190-6713)

J.A.M. ORCID (0000-0002-7494-1466)

SUMMARY

Collective cell migration is integral to many developmental and disease processes. Previously, we discovered that protein phosphatase 1 (Pp1) promotes border cell collective migration in the *Drosophila* ovary. We now report that the Pp1 phosphatase regulatory subunit dPPP1R15 is a critical regulator of border cell migration. dPPP1R15 is an ortholog of mammalian PPP1R15 proteins that attenuate the endoplasmic reticulum (ER) stress response. We show that, in collectively migrating border cells, dPPP1R15 phosphatase restrains an active physiological PERK-eIF2α-ATF4 stress pathway. RNAi knockdown of *dPPP1R15* blocks border cell delamination from the epithelium and subsequent migration, increases eIF2α phosphorylation, reduces translation, and drives expression of the stress response transcription factor ATF4. We observe similar defects upon overexpression of ATF4 or the eIF2α kinase PERK. Furthermore, we show that normal border cells express markers of the PERK-dependent ER stress response and require PERK and ATF4 for efficient migration. In many other cell types, unresolved ER stress induces initiation of apoptosis. In contrast, border cells with chronic RNAi knockdown of *dPPP1R15* survive. Together, our results demonstrate that the PERK-eIF2α-ATF4 pathway, regulated by dPPP1R15 activity, counteracts the physiological ER stress that occurs during collective border cell migration. We propose that *in vivo* collective cell migration is intrinsically "stressful", requiring tight homeostatic control of ER stress response for collective cell cohesion, dynamics, and movement.

INTRODUCTION

Collective cell migration is a fundamental component of many developmental, physiological, and pathological processes, including gastrulation, wound healing, and metastasis.[1–4] During migration, cell collectives maintain their fundamental energetic and cellular processes to remain viable and to complete their movements. Studies in diverse models have revealed how cell collectives are specified, maintained, polarized, and guided during migration.[1,3,5–8] Because of the dynamic complexity of individual cells within collectives, the entire collective, and the environments through which they move, much less is understood about homeostatic mechanisms that help cell collectives thrive and migrate *in vivo*.

Drosophila ovarian border cells represent a robust, tractable genetic model to study collective cell migration within three-dimensional (3D) tissues.[9,10] In mid-oogenesis, four to six follicle cells surround the anterior polar cell pair and are specified to become migratory border cells (Figure 1A). This border cell 'cluster' detaches (delaminates) from the follicular epithelium and migrates between large central 'nurse cells' to reach the anterior oocyte border at stage 10 (Figure 1A).[9] The migration process is energy-intensive.[11,12] Throughout migration, border cells remain associated and move cooperatively even while changing shape and position in the cluster (Figures 1B-1D). Border cells at the front further extend F-actin-rich protrusions that help the cluster to migrate effectively through the tissue.[13,14] How migrating border cells, and other cell collectives, maintain homeostasis under the energetic "loads" and associated molecular, cellular, and mechanical stresses of migration is poorly understood.

The Integrated stress response (ISR) mediates cellular responses to environmental and cellular stresses, particularly stresses that necessitate regulation of protein and membrane biosynthesis fluxes. Different stresses activate distinct kinases that phosphorylate the eukaryotic initiation factor eIF2α to reduce overall mRNA translation, promoting the restoration of homeostasis and cell survival.[15] In mammals, four stress-activated kinases, GCN2, PERK, HRI, and PKR, respectively respond to amino acid deprivation, endoplasmic reticulum (ER) stress, iron deficiency, and viral double stranded RNA.[16] Phosphorylation of eIF2α decreases overall protein synthesis, but also induces a small number of mRNAs with short upstream open reading frames (uORFs) in their 5' untranslated regions (UTRs).[17] These include mRNAs that code for the stress response transcription factor ATF4 and the *Drosophila* basic leucine zipper transcription factor Xrp1.[18,19] ATF4 itself upregulates the expression of downstream genes that help cells recover from stress.[18]

In a negative feedback loop, a protein phosphatase dephosphorylates eIF2α to attenuate stress response and promote cellular recovery. This phosphatase consists of a PP1 catalytic subunit (Pp1c) and either of two similar regulatory subunits, PPP1R15A (also termed GADD34) or PPP1R15B (also termed CReP).[20] *Drosophila* has orthologs of GCN2 and PERK but lacks orthologs of HRI and PKR. Additionally, dephosphorylation of eIF2α in *Drosophila* is carried out by a single PPP1R15-type regulatory subunit, dPPP1R15.[21] While dPPP1R15 associates with the ER, ER stress does not induce its transcription, unlike its mammalian counterparts. Nonetheless, ER stress does regulate the translation of dPPP1R15 through uORFs in the 5' UTR of the *dPPP1R15* gene.[21]

Stress-activated pathways contribute directly to cancer and metabolic disorders.[22] However, less is known about the function of these pathways during normal development and *in vivo* "baseline" cellular processes, especially complex, dynamic processes such as collective cell migration. We show here that dPPP1R5 negatively regulates the PERK-eIF2α-ATF4 ER stress response pathway in border cells. Further, we find that border cells exhibit markers of physiological ISR during normal migration. We thus identify an unexpected role for dPPP1R15 as a critical regulator of collective cell migration through restraint of an intrinsic eIF2α-ATF4 ER stress response.

RESULTS

dPPP1R15 is a Pp1 regulatory subunit required for border cell migration

Previously, we discovered that Pp1 catalytic subunits (Pp1c) promote collective versus single cell migration of border cells.[23] Pp1c binds to diverse non-catalytic regulatory subunits to form distinct Pp1 phosphatase complexes that target and dephosphorylate specific substrates.[24] Myosin phosphatase, which contains the regulatory subunit MBS (Myosin Binding Subunit) and regulates myosin activation, modulates border cell shape and movement.[23] Because additional regulatory subunits likely mediate Pp1c specificity for other substrates, we performed an RNAi screen of *Drosophila* Pp1 regulatory subunits in border cells (Figure 1E).[25–27] We drove UAS-RNAi in border cells, and in other follicle cells, using the strong *c306*-GAL4 driver (Figure S1A, S1A'). We assayed whether border cell clusters reached the oocyte by stage 10 (complete migration) or stopped along the migration pathway (incomplete migration). Among 166 RNAi lines that targeted 82 genes, 17 lines (targeting 15 genes) prevented the migration of at least 10% of border cell clusters (Table S2). Two independent lines for Inhibitor-2 (I-2) and dPPP1R15, respectively, disrupted border cell migration. While further work is needed to

confirm requirement of the 13 other genes, this screen supports the involvement of multiple Pp1 complexes in border cell migration.

We focused on *dPPP1R15* because it was reported to function in a Pp1 phosphatase complex for one substrate, eIF2α.[20] Using a fosmid reporter line, we found that dPPP1R15-GFP was ubiquitously expressed in the ovary, including in border cells (Figure S1D). Knockdown of *dPPP1R15* using independent RNAi lines strongly disrupted border cell migration, with up to 60% of clusters remaining at the anterior tip of the egg chamber (Figures 1F-1I; Figure S1C). To confirm *dPPP1R15 RNAi* specificity, we expressed wild type UAS-dPPP1R15 (Figure S1E). While co-overexpression of a control, mCD8.ChRFP, did not rescue *dPPP1R15-RNAi* migration defects, co-overexpression of dPPP1R15 fully rescued migration (Figure S1E). Overexpression of human PPP1R15B also significantly restored migration in *dPPP1R15-RNAi* egg chambers (Figure S1E).

We confirmed that dPPP1R15 functions with Pp1c in border cells (Figure S2A, S2B). Overexpression of dPPP1R15 alone severely disrupted cluster migration, cell shape, and cohesion (Figure S2C, S2F, S2G), which strongly resembled phenotypes caused by global inhibition of Pp1 phosphatase activity.[23] Overexpression of Pp1 regulatory subunits can aberrantly block general Pp1 catalytic activity, even if when normally they direct Pp1c to distinct substrates at physiological levels.[24] Overexpression of either of two dPPP1R15 mutants predicted to disrupt dPPP1R15 interaction with Pp1c [28] only mildly disrupted migration and cluster cohesion (Figure S2B, S2D-G). dPPP1R15 overexpression may impede Pp1 activity by titrating Pp1c away from other regulatory subunits, whereas mutation of these Pp1c binding sites suppressed this interference. We also co-overexpressed each of four Pp1c subunits with wild type dPPP1R15. One fly Pp1c, Pp1α-96A, as well as human hPPP1CC, significantly suppressed the dPPP1R15 overexpression defects (Figure S2H, S2I). Thus, dPPP1R15 functions as a Pp1c regulatory subunit to promote border cell delamination and migration.

dPPP1R15 promotes stable front-directed border cell protrusions and cluster polarity

In border cells that lack *dPPP1R15*, delamination from the anterior epithelium often fails (Figures 1G-I). To understand how loss of *dPPP1R15* affects cellular and subcellular features within the border cell cluster, we carried out live imaging of control and *dPPP1R15-RNAi* border cells. During migration, the leading edge of the collective forms actin-rich protrusions that provide traction for forward movement.[29] Typically, one major protrusion formed and retracted at the front of delaminating control border cell clusters (Figure 2A and 2C; Video S1). In contrast,

dPPP1R15-RNAi border cells extended significantly fewer front protrusions (Figure 2B and 2C; Video S2), decreasing from ~0.9 per frame in control to ~0.2 per frame in *dPPP1R15-RNAi* border cells (Figure 2C). While the lengths and sizes of front protrusions were not significantly different, we observed longer and larger side-directed protrusions in *dPPP1R15-RNAi* border cell clusters (Figure 2D and 2E). The movement of individual border cells also appeared to be less coordinated within *dPPP1R15-RNAi* clusters (compare Videos S1 and S2).

The disorganized protrusions and reduced coordination within *dPPP1R15-RNAi* clusters could result from disrupted cell-cell adhesion, cell polarity, or both. The adhesion protein E-cadherin is required for border cell delamination and coordinated communication for directional migration.[5,30] Normally, high levels of E-cadherin protein are present at cell-cell contacts between polar cells and border cells (Figure S3A, S3A', S3D) and between border cells (Figure S3A, S3A', S3E). Conversely, E-cadherin levels are typically low at contacts between border cells and nurse cells (Figure S3A, S3A', S3F). In *dPPP1R15-RNAi* border cell clusters, we observed typical overall patterns of E-cadherin localization (Figure S3B, B'). The levels of E-cadherin were moderately lower only at cell contacts between *dPPP1R15-RNAi* border cells, though this did not reach statistical significance (Figure S3B, S3B', S3D-F).

Next, we examined the localization of two polarity proteins, the apical marker atypical Protein Kinase C (aPKC) and the basolateral marker Discs Large (Dlg). Prior to delamination, aPKC localizes to the cluster front, particularly in a "cap" at apical polar cell membranes but also at cell membranes between border cells (Figure S3G, S3G').[31] Dlg localizes to lateral border cell membranes and to the polar cell membrane "cap" in a region more lateral than aPKC (Figure S3L, S3L').[31] *dPPP1R15-RNAi* knockdown did not affect the levels of aPKC or Dlg (Figure S3H, S3H', S3J, S3M, S3M', S3O) but disrupted the orientation of aPKC and Dlg in the polar cell cap (Figure S3G-H', S3K, S3L-M', S3P). Thus, while E-cadherin was generally normal, the polar cells appeared to be misoriented. Altogether, these data suggest that a combination of unstable protrusions, cluster disorganization, and defective cell coordination contributes to delamination failure and migration defects in *dPPP1R15-RNAi* border cell clusters.

dPPP1R15 suppresses eIF2α phosphorylation in border cells

Mammals have two orthologues of dPPP1R15, the inducible PPP1R15A and the constitutively expressed PPP1R15B, which can each partner with Pp1c. The resulting complexes dephosphorylate eIF2α at Ser 51 as part of a negative feedback loop within the integrated stress response pathway.[20] Unphosphorylated eIF2α, in combination with two other eIF2

subunits, functions as an eukaryotic initiation factor to facilitate translation initiation.[16] Phosphorylated eIF2α dissociates from the eIF2 complex and negatively regulates translation of conventional mRNAs.[32] In cultured mammalian cells, dPPP1R15 can form a complex with human Pp1c, associate with the ER, and dephosphorylate eIF2α.[21] We investigated whether *dPPP1R15* regulates eIF2α phosphorylation in border cells using an antibody that recognizes Ser 51-phosphorylated eIF2α (p-eIF2α). We measured and normalized p-eIF2α levels to Singed (Sn; *Drosophila* Fascin), a uniformly cytoplasmic protein in border cells (Figure S4A-C). In control border cells, p-eIF2α was barely detectable (Figure 3A-A", 3C; Figure S4A, S4A', S4C). Upon *dPPP1R15-RNAi* knockdown, p-eIF2α was significantly increased (Figure 3B-C; Figure S4B-C). This effect was specific to phosphorylated eIF2α because total eIF2α protein levels were unchanged (Figure S4E-F', S4I).

We next investigated the relationship between eIF2α phosphorylation and the migration defects caused by *dPPP1R15-RNAi* knockdown. We generated UAS-eIF2α wildtype ($eIF2\alpha^{WT}$), non-phosphorylatable mutant ($eIF2\alpha^{S51A}$), and phosphomimetic mutant ($eIF2\alpha^{S51D}$) lines. Overexpression of $eIF2\alpha^{WT}$ or $eIF2\alpha^{S51A}$ had no effect on border cell migration (Figure 3D, 3E, 3G; Figure S4H, S4H'). However, ectopic expression of phosphomimetic $eIF2\alpha^{S51D}$ resulted in a significant migration defect (Figure 3F, 3G). We introduced the three forms of eIF2α into the *dPPP1R15-RNAi* background. $eIF2\alpha^{WT}$ and $eIF2\alpha^{S51A}$ partially rescued the migration defects caused by *dPPP1R15* knockdown, compared to a control construct (mCD8.ChRFP; Figure 3H). In contrast, phosphomimetic $eIF2\alpha^{S51D}$ did not rescue the migration defects (Figure 3H). These results confirm that dPPP1R15 regulates eIF2α activity in border cells.

dPPP1R15 suppresses PERK-mediated ER stress signaling in border cells

In *Drosophila*, two distinct kinases, PERK and GCN2, phosphorylate eIF2α as part of the integrated stress response pathway (Figure 4A).[21,33] We investigated whether dPPP1R15 counteracts one or both of these kinases by overexpressing PERK or GCN2 in border cells. As PERK overexpression with *c306*-GAL4 was lethal, we drove high levels of UAS-PERK in border cells using the more restricted *slbo*-GAL4 (Figure 4B-E; Figure S1B, S1B'). Strikingly, at the stage in which control border cells normally reach the oocyte (Figure 4B, 4E), most PERK-overexpressing border cell clusters failed to delaminate (Figure 4C, 4E). This strong effect of PERK depends on its kinase activity, as overexpression of a kinase-dead mutant (K671R, "PERK-KD") resulted in milder migration defects (Figure 4D, 4E). Levels of p-eIF2α, but not total eIF2α, were significantly higher in PERK-expressing border cells compared to PERK-KD or

control border cells (Figure 4F-H; Figure S4D, S4G, S4G', S4I). As observed in fixed tissue (Figure 4C, 4E), live-imaged PERK-overexpressing border cells did not delaminate (Figure S5; Video S3). Although individual border cells were motile within the cluster, only small transient protrusions formed in PERK-overexpressing border cells (Figure S5; Video S3). We observed significant reduction of E-cadherin at border cell-border cell contacts as well as misoriented aPKC and Dlg in polar cells (Figure S3C-F, S3I-K, S3N-P). Though somewhat stronger, the border cell delamination, protrusion, and cluster adhesion and polarity phenotypes caused by PERK overexpression closely resembled the *dPPP1R15-RNAi* phenotypes.

We could not determine the effects of activated GCN2 because overexpression was lethal with *c306*-GAL4 as well as with *slbo*-GAL4.[34] Instead, we investigated whether knockdown of either *PERK* or *GCN2* rescued the migration of *dPPP1R15-RNAi* border cells. Knockdown of *PERK* by either of two RNAi lines significantly ameliorated *dPPP1R15-RNAi* border cell migration defects compared to control *mCherry-RNAi* (Figure 4I). In contrast, knockdown of *GCN2* using two independent RNAi lines did not suppress *dPPP1R15-RNAi* induced migration defects; one *GCN2-RNAi* line even enhanced the migration defects (Figure 4I). *GCN2* knockdown by itself disrupted border cell migration (Figure S6A), although levels of p-eIF2α were unaffected (Figure S6B). Thus, in border cells, dPPP1R15 functions in a PERK-dependent pathway but is independent of GCN2.

Unfolded or misfolded proteins in the ER trigger the unfolded protein response (UPR), which is mediated by several distinct branches including PERK- and IRE1-dependent pathways.[35] To determine specificity of dPPP1R15, we examined IRE1 activity with Xbp1-GFP, a reporter of IRE1-dependent Xbp1 mRNA splicing.[36] Control border cells had low levels of Xbp1-GFP that were unaffected by *dPPP1R15-RNAi* knockdown (Figure S6C-E). UPR can be induced by knocking down Sarco/endoplasmic reticulum Ca(2+)-ATPase (SERCA), which maintains calcium homeostasis in the ER to facilitate protein folding.[37] Knockdown of *SERCA* was previously shown to disrupt border cell migration without inducing IRE1-dependent Xbp1-GFP.[38] However, p-eIF2α levels in *SERCA-RNAi* were similar to control (Figure S6F-H), suggesting that Ca^{2+} homeostasis via SERCA does not induce the PERK-dependent UPR pathway in border cells. These data support specific dPPP1R15 function in the PERK-dependent ISR.

dPPP1R15 promotes global protein synthesis and inhibits ATF4 in border cells

Phosphorylation of eIF2α inhibits its activity as a general translation initiation factor, reducing global protein synthesis.[16,22] Since p-eIF2α increases in border cells upon *dPPP1R15* knockdown (Figure 3B-C), we investigated whether mRNA translation was altered. We used an O-propargyl-puromycin (OPP) Click chemistry assay to label nascent proteins in cells.[39,40] We incubated live egg chambers with OPP before fixation, labeling, and imaging (Figure 5A-B', 5D-E'). Both *dPPP1R15-RNAi* knockdown and overexpression of PERK significantly decreased the OPP signal compared to controls (Figure 5A-F), consistent with dPPP1R15 supporting general protein synthesis via eIF2α dephosphorylation in border cells.

Phosphorylation of eIF2α enhances translation of select mRNAs including the transcription factor ATF4, which drives expression of stress response genes.[18,22] Previous work showed that *ATF4* (*Drosophila cryptocephal*; *crc*) mRNA is highly expressed in border cells.[41] However, border cells exhibit low levels of an endogenous ATF4-GFP protein reporter (Figure 5G; *see* Figure 6B-C).[42] Upon *dPPP1R15* knockdown, we observed high levels of ATF4-GFP (Figure 5H). Furthermore, ATF4 overexpression significantly impaired border cell migration (Figure 5I-K). Correspondingly, *ATF4-RNAi* knockdown strongly suppressed the migration defects caused by *dPPP1R15-RNAi* (compare Figure 5L to Figure 1I). We conclude that, through its regulation of eIF2α phosphorylation, dPPP1R15 effectively restrains ATF4 protein expression in border cells.

Border cells exhibit physiological ER stress response

Do border cells experience physiological ER stress during normal delamination and collective migration? To address this question, we analyzed multiple markers of the PERK branch of the ISR pathway in otherwise unperturbed border cells (Figure 6A-J). Border cells exhibited modest ATF4 protein (ATF4-GFP reporter) levels above non-specific background (w^{1118}; Figure 6A-C). The transcription factor Xrp1 is downstream of PERK and p-eIF2α but independent of ATF4 in some tissues.[19] Normal border cells expressed significant levels of Xrp1-GFP, a reporter of Xrp1 protein, and Xrp1-lacZ, a reporter of Xrp1 transcript [43] (Figure 6D-F, 6I-J). We also analyzed expression of the *Drosophila* eIF4E-Binding (4E-BP) protein Thor, a known transcriptional target of ATF4.[36] Expression of Thor-lacZ was significantly above background levels in border cells (Figure 6G-H', 6J). Thus, multiple markers of the PERK-dependent ISR pathway are intrinsically expressed in normal border cells.

We next probed the consequences of inhibiting the ER stress response pathway in border cells. RNAi knockdown of either *PERK* or *ATF4* driven by *c306*-GAL4 inhibited migration in ~20-30% of egg chambers (Figure 6K-L). One *PERK-RNAi* line and one *ATF4-RNAi* line exhibited mild migration defects when knockdown was induced for 1-day (Figure 6K) but had significantly increased migration defects when induced for 3-days (Figure 6L). We conclude that loss of the ER stress response disrupts border cell migration. These data suggest that border cells experience intrinsic physiological ER stress, which is counteracted by the PERK-eIF2a-PPP1R15 pathway to maintain normal delamination and collective cell migration.

Loss of *dPPP1R15* does not induce apoptosis of border cells

Failure to resolve ER stress can trigger pro-apoptotic pathways.[44,45] Therefore, we investigated whether dPPP1R15 is required for border cell survival (Figure 7). We drove *dPPP1R15-RNAi* in anterior/posterior follicle cells and border cells throughout oogenesis using *c306*-GAL4 (Figure 7A) and analyzed the expression of the apoptotic marker cleaved death caspase-1 (cDCP-1).[44] Early in oogenesis, extra polar cells form but undergo regulated apoptosis; after stage 6, only two polar cells remain at anterior and posterior poles of egg chambers.[46] We observed cDCP-1+ staining in polar cells of stage 6 control and *dPPP1R15-RNAi* egg chambers, consistent with normal cell death patterns (Figure 7B, 7C). Similarly, we did not detect cDCP-1 in either control or *dPPP1R15-RNAi* border cells or other follicle cells at later stages (Figure 7D, 7E). To mimic chronic ER stress, we extended *dPPP1R15-RNAi* knockdown from one day to three days ("3 days RNAi"). While control stage 6 anterior polar cells exhibited normal cDCP-1 patterns (Figure 7F), prolonged *dPPP1R15-RNAi* dramatically increased the number of cDCP-1+ cells (Figure 7G). Nevertheless, at later stages, we did not detect cDCP-1+ signal in border cells or follicle cells in either control or *dPPP1R15-RNAi* egg chambers (Figure 7H, 7I). We next expressed p35, a baculoviral inhibitor of proapoptotic caspases. Co-expression of p35, a baculoviral inhibitor of proapoptotic caspases [47], had no significant effect on *dPPP1R15-RNAi* migration defects (Figure 7J). Thus, the *dPPP1R15-RNAi* border cell delamination and migration defects are likely caused by elements of the stress response pathway unrelated to the apoptotic cascade.

DISCUSSION

Uncontrolled ER stress along with the UPR is implicated in diseases ranging from type I diabetes to neurodegenerative diseases and cancer.[22,35,48] However, some cells and tissues

exhibit intrinsic stress signaling under non-pathological conditions. These include cells with high metabolic activity, such as adipocytes and liver cells, and secretory cells, such as pancreatic β-cells and mammary gland cells.[49,50] *PERK*, *PPP1R15,* and *ATF4* are required for tissue and organ development and for organismal viability.[22,42,51,52] Olfactory receptor neurons also require a PERK-dependent ER stress response to upregulate the expression of genes that target axons to specific positions.[53] In migrating cells, however, roles for UPR and ER stress are less defined and depend on cellular type and context.[54] Much of the available data comes from studies on single cell migration in pathological contexts.[54–56] For example, cancer cells undergoing epithelial-mesenchymal transitions exploit hyperactivated ER stress responses to promote migration, invasion and metastasis.[56] Compared to individually migrating cells, functions of the ER stress pathway and other stress pathways in collective cell migration, especially in native contexts, are even less understood.

Our results support a model in which intrinsic physiological ER stress in normal border cells is actively restrained by dPPP1R15 to limit the PERK-p-eIF2α ER stress response (Figure 7K, 7L). This allows the cluster to polarize, form stable front-directed protrusions, delaminate, and successfully migrate. How does dPPP1R15-mediated restraint of the ER stress pathway contribute to border cell collective migration? Moreover, what are the molecular drivers of intrinsic stress signaling in collectively migrating border cells? One possibility is that unusually high or stringent requirements for membrane protein biogenesis cause intrinsic ER stress that must be counteracted by dPPP1R15. Border cells express high levels of many transmembrane glycoproteins that are mobilized for collective migration, including adhesion proteins and gap junction proteins.[30,57] Some of these proteins regulate delamination and protrusions in border cells, processes that are strongly perturbed by aberrant ER stress signaling. E-cadherin, a major adhesion membrane glycoprotein, is highly expressed just prior to border cell formation and is essential for migration.[30] Delamination itself requires remodeling of E-cadherin-based cell adhesions between border cells and adjacent follicle cells, along with localized actomyosin contraction of the entire border cell cluster.[7,9] We showed that PERK overexpression significantly reduced the levels of E-cadherin. Thus, high levels of E-cadherin biogenesis may be a source of physiological ER stress in border cell migration. Other membrane proteins required for border cell formation, delamination, and anchoring to the oocyte, such as the transmembrane receptor Notch and its ligand Delta or gap junction proteins, may also contribute.[57]

In addition to its role in membrane protein biogenesis, the ER is a source of membrane lipids and phosphoinositides. Formation of front-directed protrusions and cellular shape changes during migration draw upon both bulk membrane and specific membrane lipid components.[58,59] However, these requirements may also contribute to ER stress through so-called “lipid bilayer stress” mechanisms.[60] Finally, collective cell migration is energetically expensive.[11,12] Stresses could result from the complex interplay between mitochondria, reactive oxygen species generated during mitochondrial function, calcium homeostasis, and the oxidative and calcium loading status of the ER lumen.[61]

Cells with unresolved chronic ER stress can undergo apoptosis.[45] Persistent knockdown of *dPPP1R15* induced apoptosis of early follicle cells but not border cells. These results raise the intriguing possibility that border cells are more resistant to ER stress-induced apoptosis than follicle cells. While the apoptotic inhibitor Death-associated inhibitor of apoptosis 1 (DIAP1) is expressed in mid-oogenesis, DIAP1 is required for Rac-mediated border cell migration independent of its roles in apoptosis.[62] Border cells may express other proteins that inhibit cell death, or have a low complement of proteins that activate apoptosis in response to ER stress. Mammalian ER stress-dependent cell death occurs primarily due to activation of the transcription factor C/EBP homologous protein (CHOP), which promotes expression of apoptotic genes.[45] *Drosophila* lacks a direct homolog of CHOP, though prolonged ER stress induces cell death via PERK-ATF4 in wing imaginal discs.[40,63] The molecular basis for the resistance of border cells to ER stress-induced cell death remains to be characterized.

Independent of the nature of specific molecular drivers of border cell ER stress, our results suggest that dPPP1R15 responds to changes in eIF2α phosphorylation to establish a setpoint of ISR (Figure 7K, 7L). dPPP1R15 also restores baseline mRNA translation and cell health after acute transient stresses that may occur at specific points in the delamination and collective migration process. Optimal levels of the PPP1R15 phosphatase thus restrain the PERK-eIF2α-ATF4 ER stress response pathway for successful collective movement. The notable similarities between collective border cell migration and other migrating and invading collectives in human development and cancer suggest that these mechanisms may be broadly conserved.[1,64]

ACKNOWLEDGEMENTS

We thank Denise Montell, Deepika Vasudevan, Hyung Don Ryoo, the Bloomington Drosophila Stock Center, the Developmental Studies Hybridoma Center (University of Iowa), the Drosophila

Genomics Resource Center (NIH Grant 2P40OD010949), the Zurich ORFeome Project (FlyORF), and the Vienna Drosophila Resource Center (VDRC) for fly stocks, cDNAs, plasmids, antibodies, and protocols. We are especially thankful to Deepika Vasudevan and Lydia Grmai for discussion of results prior to publication. We also thank Saurav Misra, Emily Burghardt, and Rehan Khan for helpful discussions and providing critical comments on the manuscript. The Confocal Core, funded by the Kansas State University College of Veterinary Medicine, provided use of the Zeiss LSM 880 confocal microscopes. This work was supported in part by a fellowship from the Kansas INBRE through the National Institutes of Health (P20 GM103418) to Y.C., and by a grant from the National Science Foundation (NSF 2027617) to J.A.M.

AUTHOR CONTRIBUTIONS

Y.C.: Conceptualization, Formal analysis, Funding acquisition, Validation, Investigation, Visualization, Methodology, Writing – original draft, Writing – review & editing; J.A.M.: Conceptualization, Supervision, Funding acquisition, Methodology, Writing – original draft, Writing – review & editing.

DECLARATION OF INTERESTS

The authors declare no competing interests.

FIGURE LEGENDS

Figure 1. *dPPP1R15* is required for border cell migration

(A) Illustration of border cell migration.

(B-D) Representative images of border cell migration (arrowheads) in egg chambers labeled with E-Cadherin (E-cad; red) and DAPI (blue). Insets, magnified border cell clusters.

(E) Outline of Pp1 regulatory subunit *RNAi* screen.

(F-H) *dPPP1R15-RNAi* knockdown causes border cell migration defects; border cells labeled by Singed (SN, green); F-actin (magenta) and DAPI (blue) label all cells.

(I) Quantification of migration for matched control and *dPPP1R15-RNAi*, shown as percentage of complete (green), delayed (orange), and no (blue) migration. Error bars represent standard deviation (SD) from 3 experiments; each trial assayed n ≥ 43 egg chambers (total n ≥ 144 egg chambers per genotype); **p < 0.01, ***p < 0.001, unpaired two-tailed *t* test.

UAS-*RNAi* driven with *c306*-Gal4. Scale bars, 50 μm (B-D, F-H).

See also Figures S1 and S2 and Tables S1 and S2.

Figure 2. *dPPP1R15* promotes normal border cell protrusion dynamics

(A and B) Frames from control (Video S1) and *dPPP1R15-RNAi* (Video S2) egg chambers showing migrating border cells; cell membranes labeled with PLCδ-PH-EGFP. Time in min. Arrows indicate protrusions.

(C-E) Quantification of protrusion dynamics: number per frame (C), average length (D), and average area (E) from videos. Control protrusions measured in 13 videos (n = 13 front-directed protrusions, n = 4 side-directed protrusions); *dPPP1R15-RNAi* protrusions measured in 15 videos (n = 6 front protrusions, n = 4 side protrusions). Diagrams illustrate protrusion direction. Data presented as box-and-whisker Split Violin Plots. **p<0.01, unpaired two-tailed *t* test.

UAS-*RNAi* driven with *c306*-Gal4. Scale bars, 5 μm (A, B).

See also Figure S3, Table S1, and Videos S1 and S2.

Figure 3. dPPP1R15 suppresses eIF2α phosphorylation in border cells

(A-B'') Representative images showing p-eIF2α staining in *mCherry* (A-A'') or *dPPP1R15* (B-B'') *RNAi* knockdown border cells.

(C) Quantification of normalized p-eIF2α intensity in border cells; n = 21 for control *mCherry-RNAi*; n = 33 for *dPPP1R15-RNAi*; ****p<0.0001, unpaired two tailed *t* test.

(D-G) Overexpressing eIF2α-S51D (F), but not eIF2α-WT (D) or eIF2α-S51A (E) disrupted border cell migration. (G) Quantification of border cell cluster migration defects for control (mCD8.ChRFP) and eIF2α WT and mutants, shown as percentage of complete (green), delayed (orange), and no (blue) migration. Error bars represent SD from 3 experiments; each trial assayed n ≥ 60 egg chambers (total n ≥ 184 egg chambers per genotype); *p<0.05, **p<0.01, one-way ANOVA followed by Dunnett's multiple comparisons test.

(H) Overexpressing eIF2α-WT or eIF2α-S51A but not eIF2α-S51D partially restores *dPPP1R15-RNAi* migration defects. Error bars represent SD from 3 experiments; each trial assayed n ≥ 72 egg chambers (total n ≥ 250 egg chambers per genotype), ***p<0.001, one-way ANOVA followed by Dunnett's multiple comparisons test.

UAS-*RNAi* and overexpression driven with *c306-Gal4.* Scale bars, 50 μm (A, B, D-F) and 10 μm (A', A'', B', B'').

See also Figure S4 and Table S1.

Figure 4. dPPP1R15 suppresses PERK-mediated stress signaling in border cells

(A) Schematic depiction of *Drosophila* eIF2α kinases.

(B-D) Representative stage 10 egg chambers showing border cells (arrowheads) overexpressing lacZ (control, B), PERK (C), or PERK-KD (D).
(E) Quantification of migration defects upon lacZ, PERK or PERK-KD overexpression. Error bars represent SD from 3 experiments; each trial assayed n ≥ 34 egg chambers (total n ≥ 118 egg chambers per genotype); ****p<0.0001, one-way ANOVA followed by Dunnett's multiple comparisons test.
(F-G') PERK overexpression promotes p-eIF2α levels in border cells.
(H) Quantification of p-eIF2α levels; n = 14 control (lacZ), n = 15 PERK overexpression; **p<0.01, unpaired two tailed *t* test.
(I) *PERK-RNAi* but not *GCN2-RNAi* partially suppressed *dPPP1R15-RNAi* migration defects. Error bars represent SD from 3 experiments; each trial assayed n ≥ 58 egg chambers (total n ≥ 232 egg chambers per genotype); *p<0.05, one-way ANOVA followed by Dunnett's multiple comparisons test.
UAS-*RNAi* driven with *c306*-Gal4; overexpression driven with *slbo*-Gal4. Scale bars, 50 μm (B-D) and 10 μm (F-G').
See also Figures S3-S6, Table S1, and Video S3.

Figure 5. dPPP1R15 promotes global protein synthesis and inhibits ATF4 in border cells
(A-F) Global protein synthesis levels visualized by O-propargyl-puromycin (OPP, green) in border cells (SN, red). Representative examples of lacZ control (A, A'), PERK overexpression (B, B'), *mCherry-RNAi* control (D, D'), and *dPPP1R15-RNAi* (E, E'). (C, F) Quantification of normalized average OPP intensity. (C) n = 10 for lacZ control, n = 10 for PERK overexpression. (D) n = 10 for *mCherry-RNAi* control, n = 11 for *dPPP1R15-RNAi*. ***p < 0.001, ****, p<0.0001, unpaired two-tailed t test.
(G, H) ATF4-GFP protein in control *mCherry-RNAi* (G) versus *dPPP1R15-RNAi* (H) border cells.
(I-J) Border cell migration (arrowheads) in mCD8.RFP control (I) versus ATF4 overexpression (J).
(K) Quantification of migration defects upon mCD8.RFP or ATF4 (two independent lines) overexpression. Error bars represent SD from 3 experiments; each trial assayed n ≥ 88 egg chambers (total n ≥ 331 egg chambers per genotype); ***p < 0.001, unpaired two-tailed *t* test.
(L) *ATF4-RNAi* partially restores migration defects induced by *dPPP1R15-RNAi*. Error bars represent SD from 3 experiments; each trial assayed n ≥ 79 egg chambers (total n ≥ 265 egg chambers per genotype); **p < 0.01, unpaired two-tailed *t* test.

PERK and lacZ overexpression driven with *slbo*-Gal4; other UAS-lines driven with *c306*-Gal4. Scale bars, 10 μm (A-B', D-E', G, H) and 50 μm (I, J).
See also Table S1.

Figure 6. Border cells exhibit physiological ER stress response
(A-F) ATF4-GFP (B, B') and Xrp1-GFP (E, E') expression in normal border cells (arrowheads). w^{1118} border cells (A, A' and D, D'), without reporters, demonstrates GFP antibody specificity. (C, F) Quantification of GFP intensity. (C) n = 12 for w^{1118}, n = 14 for ATF4-GFP. (F) n = 11 for w^{1118}, n = 11 for Xrp1-GFP. **p<0.01, unpaired two tailed *t* test.
(G-J) Thor-lacZ (H, H') and Xrp1-lacZ (I, I') expression in normal migrating border cells (arrowheads). (G, G') w^{1118}, without lacZ, demonstrates lacZ antibody specificity. (J) Quantification of lacZ intensity; n = 10 for w^{1118}, n = 9 for Thor-lacZ, n = 10 for Xrp1-lacZ; ****, p<0.0001, one-way ANOVA followed by Dunnett's multiple comparisons test.
(K and L) Quantification of migration defects for *mCherry-RNAi*, *PERK-RNAi* and *ATF4-RNAi* in 1-day *RNAi* (K) or 3-day *RNAi* (L) conditions (29˚C). Error bars represent SD from 3 experiments; each trial assayed n ≥ 38 egg chambers (total n ≥ 121 egg chambers per genotype); *p<0.05, **p<0.01, ***p < 0.001, one-way ANOVA followed by Dunnett's multiple comparisons test.
UAS-*RNAi* driven with *c306*-Gal4. Scale bars, 10 μm (A-B', D-E', G-I').
See also Table S1.

Figure 7. Loss of *dPPP1R15* does not induce apoptosis of border cells
(A) Ovariole showing *c306*-GAL4 pattern (mcD8.ChRFP; red) from germarium through stage 10. F-actin (green), cell membranes; DAPI (blue), cell nuclei.
(B-E) 1-day *RNAi* conditions. (B, C) Normal patterns of cDCP-1+ cells (arrowheads) during early oogenesis in control (*mCherry-RNAi*; B) and *dPPP1R15-RNAi* (C). (D, E) Control (*mCherry-RNAi*; D) and *dPPP1R15-RNAi* (E) border cells (dotted lines) do not express cDCP-1.
(F-I) 3-day *RNAi* conditions. (F) Normal cDCP-1+ (arrowhead) cell in a control egg chamber. (G) Ectopic cDCP-1+ in follicle cells (bracket) in a *dPPP1R15-RNAi* egg chamber. (H, I) Control (H) and *dPPP1R15-RNAi* (I) border cells (dotted lines) and anterior follicle cells (arrowhead) do not express cDCP-1.
(J) p35 overexpression does not rescue *dPPP1R15-RNAi* border cell migration defects. Error bars represent SD from 3 experiments; each trial assayed n ≥ 56 egg chambers (total n ≥ 267 egg chambers per genotype); unpaired two-tailed *t* test.

(K and L) Models for dPPP1R15 and ER stress response pathway functions in normal border cell migration (K) and in excessive ER-stress conditions (L).
c306-Gal4 was used to drive UAS-*lines*. Scale bars, 50 μm (A-C) and 10 μm (D-I).
See also Table S1.

STAR METHODS

RESOURCE AVAILABILITY

Lead Contact

Further information and requests for resources and reagents should be directed to and will be fulfilled by the lead contact, Jocelyn McDonald (jmcdona@ksu.edu)

Materials Availability

New *Drosophila* lines and plasmids generated in this study are available by request to the Lead Contact above.

Data and Code Availability

- All data reported in this paper will be shared by the lead contact upon request.
- This paper does not report original code.
- Any additional information required to reanalyze the data reported in this paper is available from the lead contact upon request.

EXPERIMENTAL MODEL AND SUBJECT DETAILS

Drosophila genetics and strains

Standard cornmeal-yeast food was used in this study. Most flies and crosses were kept in incubators at 25℃ unless indicated otherwise. The key resources table contains a detailed list of all fly strains used in this study and their sources. Each figure panel's genotypes are listed in Table S1. Most flies were fattened by yeast addition overnight at 29℃ before dissection. The exceptions were for some RNAi experiments, in which flies were incubated for 3 days at 29℃.

METHOD DETAILS

Generation of fosmid and UAS transgenic lines

The dPPP1R15 fosmid construct was acquired from the Drosophila TransgeneOme (https://transgeneome.mpi-cbg.de/) and the transgenic fly was created by the GenetiVision Corporation (Houston, Texas) according to described methods.[65] The coding regions of wild-type dPPP1R15 and eIF2α were cloned from cDNAs. All the mutants of dPPP1R15 and eIF2α were generated through the Phusion Site-Directed Mutagenesis Kit and verified by sequencing (Eton Bioscience Inc.). Once generated, the mutant cDNAs were cloned into the pUASg-HA-attB vector using Gateway technology. Fly injections were performed by GenetiVision Corporation using the PhiC31-based Transgenesis System. The dPPP1R15 WT and corresponding mutants were inserted into the P2(3L)68A4 site; the eIF2α WT and the corresponding mutants were inserted into the VK20(3R)99F8 site.

Immunostaining

Fly ovaries from 3- to 5-d-old females were dissected in Schneider's Drosophila Medium (Thermo Fisher Scientific, Waltham, MA, USA) supplemented with 10% fetal bovine serum (Seradigm FBS; VWR, Radnor, PA, USA). Ovaries were kept whole or dissected into individual egg chambers, followed by fixation for 10 min using 4% methanol-free formaldehyde (Polysciences, Warrington, PA, USA) in 0.1 M potassium phosphate buffer, pH 7.4, or in 1X Phosphate Buffered Saline (PBS). Washes and antibody incubations were performed in 'NP40 block' (50 mM Tris-HCl, pH 7.4, 150 mM NaCl, 0.5% NP40, 5 mg/ml bovine serum albumin [BSA]). The key resources table contains a detailed list of all antibodies used in this study and their sources.

In vivo protein synthesis assay

Ovaries from 10-15 flies were dissected in live imaging medium (1 × Schneider's Drosophila medium, 20% FBS, 0.2 mg/mL insulin, 1 × antibacterial-antimycotic solution, pH 6.95) and transferred into live imaging medium with 20μM Click-iT OPP reagent. Dissected egg chambers were then incubated at room temperature for 30 min and rinsed one time with 1x PBS. Samples were then fixed with 4% paraformaldehyde in PBS for 20 min, rinsed three times with 1x PBS and subsequently washed in 1x PBST (1X phosphate-buffered saline, 0.1% Triton X-100) and 1x PBS with 3% BSA for 10 min. Click reactions were performed in the dark at room temperature for 30 min. Samples were washed once with the rinse buffer provided by the Click-iT reaction kit and three times with 1x PBST, then were incubated in 1x PBST at room

temperature for 1 hr. Primary antibodies were added and incubated with the egg chambers at 4℃ overnight. Samples were rinsed three times with 1x PBST and incubated in 1x PBST at room temperature for 1 hr. Nuclear Mask reagent (1:2000) and secondary antibodies (1:400) were added in 1x PBST and incubated with egg chambers at room temperature for 2 hr. Samples were then rinsed three times with 1x PBST and incubated for 2 hr.

Microscopy and live time-lapse imaging

Images of fixed egg chambers were acquired with an upright Zeiss AxioImager Z1 microscope, or on a Zeiss LSM 880 confocal microscope with or without Airyscan (KSU College of Veterinary Medicine Confocal Core), using either a 20x 0.75 numerical aperture (NA) or 40x 1.3 NA oil-immersion objective. Live time-lapse imaging was performed as described [66] with a modification to the mounting procedure.[67] Briefly, ovarioles were dissected in room-temperature sterile live imaging media (Schneider's Drosophila Medium, pH 6.95, with 15–20% FBS). Fresh live imaging media, supplemented with 0.2 mg/ml bovine insulin (Cell Applications, San Diego, CA, USA), was added to the sample prior to mounting on a Lumox dish 50 (94.6077.410; Sarstedt, Newton, NC, USA). After rinsing the egg chambers with 100 µl of live imaging medium, the live imaging medium was removed. The samples were rinsed with live imaging media supplemented with 100 µl fibrinogen (10 mg/mL), 10 µL fibrinogen (10 mg/mL) was added, and the egg chambers were transferred to the Lumox dish. 1 µL thrombin (10 U/mL) was added to form a fibrinogen-thrombin clot to keep the egg chambers immobilized. Time-lapse videos were generally acquired at intervals of 3 min for at least 1 hr using a 40x 1.2 NA water-immersion objective. In some cases, multiple z-stacks were acquired and merged in Zeiss ZEN, or FIJI [68] to produce a single, in-focus image or time-lapse video.

Figures and graphs

Figures were assembled in Affinity Designer (Serif, Nottingham, United Kingdom). Illustrations were created in Affinity Designer. Videos were assembled in FIJI. Graphs were created using Jupyter Notebook, Seaborn, Python.

QUANTIFICATION AND STATISTICAL ANALYSIS

Image measurements and editing were performed using Zeiss ZEN or FIJI. Analysis of live border cell migration time-lapse videos was performed using FIJI.

Quantification of protrusions was performed as described.[69] Briefly, a circle was drawn around the cell cluster, and cellular extensions greater than 1.5 mm outside the circle were defined as protrusions. Protrusions were classified as directed to the front (0˚–45˚ and 0˚–315˚), side (45˚–135˚ and 225˚–315˚), or back (135˚–225˚), based on their positions within the cluster. The first 1 hr of each video was used to quantify protrusions.

Quantifications of GFP, lacZ, p-eIF2alpha, eIF2alpha, E-Cadherin, aPKC, and Dlg intensity were performed on egg chambers stained using identical conditions for the control and experimental groups. Samples were imaged with a 40x 1.3 NA oil objective. Identical confocal laser settings were used for each channel. For measurements of E-Cadherin, aPKC, and Dlg, a z-stack of the cluster was produced (10 z-focal planes above and 10 z-focal planes below the center, for a total of 21 z-sections including the center focal plane itself). Polar cell-border cell (PC:BC), border cell-border cell (BC:BC) contacts, and nurse cell-nurse cell (NC:NC) contacts were manually identified, then a line (width set as 10) was drawn, and the mean fluorescence intensity across the line was obtained using the 'measure' tool. A ratio of PC-BC (BC-BC or BC-NC) intensity versus NC-NC intensity was calculated to normalize E-cadherin or Dlg protein levels. For measurements of GFP and lacZ levels, the mean fluorescence intensity was normalized to DAPI. For p-eIF2alpha and eIF2alpha levels, the mean fluorescence intensity was normalized to SN.

To quantify the OPP intensity, a maximum z-stack image was created. Once the center of the cluster was defined, four z-focal planes above and four z-focal planes below the center were selected, for a total of 9 z-sections including the center focal plane itself. For *dPPP1R15-RNAi* and control RNAi, the OPP intensity of the border cell cluster was measured and divided by the OPP intensity from a square (50 pixels x 50 pixels) in the cytoplasm of an adjacent nurse cell. Similar measurements of relative OPP intensity in the PERK overexpression and control were performed, except the square was drawn as 20 pixels x 20 pixels.

All statistical tests were performed using GraphPad Prism 7 or Prism 8 (GraphPad Software, San Diego, CA, USA). The statistical methods and p values are listed in the figure legends.

Table S2. Results of RNAi screen, Related to Figure 1. Complete results of the PP1 regulatory subunit RNAi survey of border cell migration (Excel file).

SUPPLEMENTAL VIDEO TITLES AND LEGENDS

Video S1. Normal border cell delamination and early migration, Related to Figure 2

Control (*c306*-GAL4, tsGAL80/+; UAS-PLCδ-PH-EGFP/+) egg chamber showing normal border cell migration.

Frames were acquired every 3 min with a 40x water immersion objective. Anterior is to the left.

Video S2. Knocking down *dPPP1R15* prevents delamination and disrupts protrusions, Related to Figure 2

dPPP1R15-RNAi (*c306*-GAL4, tsGAL80/+; UAS-dPPP1R15-RNAi/+; UAS-PLCδ-PH-EGFP/+) egg chamber showing the migration defect.

Frames were acquired every 3 min with a 40x water immersion objective. Anterior is to the left.

Video S3. PERK overexpression disrupts border cell delamination, Related to Figure 4

PERK overexpressing (*slbo*-GAL4/+; UAS-PLCδ-PH-EGFP/UAS-PERK) egg chamber showing the migration defect.

Frames were acquired every 3 min with a 40x water immersion objective. Anterior is to the left.

REFERENCES

1. Scarpa, E., and Mayor, R. (2016). Collective cell migration in development. Journal of Cell Biology *212*, 143–155. 10.1083/jcb.201508047.

2. Cheung, K.J., and Ewald, A.J. (2016). A collective route to metastasis: Seeding by tumor cell clusters. Science *352*, 167–169. 10.1126/science.aaf6546.

3. Friedl, P., and Gilmour, D. (2009). Collective cell migration in morphogenesis, regeneration and cancer. Nat Rev Mol Cell Biol *10*, 445–457. 10.1038/nrm2720.

4. Wang, X., Enomoto, A., Asai, N., Kato, T., and Takahashi, M. (2016). Collective invasion of cancer: Perspectives from pathology and development: Collective invasion of cancer. Pathology International *66*, 183–192. 10.1111/pin.12391.

5. Cai, D., Chen, S.-C., Prasad, M., He, L., Wang, X., Choesmel-Cadamuro, V., Sawyer, J.K., Danuser, G., and Montell, D.J. (2014). Mechanical feedback through E-cadherin promotes direction sensing during collective cell migration. Cell *157*, 1146–1159. 10.1016/j.cell.2014.03.045.

6. Wang, X., He, L., Wu, Y.I., Hahn, K.M., and Montell, D.J. (2010). Light-mediated activation reveals a key role for Rac in collective guidance of cell movement in vivo. Nat Cell Biol *12*, 591–597. 10.1038/ncb2061.

7. Majumder, P., Aranjuez, G., Amick, J., and McDonald, J.A. (2012). Par-1 controls myosin-II activity through myosin phosphatase to regulate border cell migration. Curr Biol *22*, 363–372. 10.1016/j.cub.2012.01.037.

8. McDonald, J.A., Pinheiro, E.M., Kadlec, L., Schupbach, T., and Montell, D.J. (2006). Multiple EGFR ligands participate in guiding migrating border cells. Developmental Biology *296*, 94–103. 10.1016/j.ydbio.2006.04.438.

9. Montell, D.J., Yoon, W.H., and Starz-Gaiano, M. (2012). Group choreography: mechanisms orchestrating the collective movement of border cells. Nat Rev Mol Cell Biol *13*, 631–645. 10.1038/nrm3433.

10. Saadin, A., and Starz-Gaiano, M. (2016). Circuitous Genetic Regulation Governs a Straightforward Cell Migration. Trends in Genetics *32*, 660–673. 10.1016/j.tig.2016.08.001.

11. DeWane, G., Salvi, A.M., and DeMali, K.A. (2021). Fueling the cytoskeleton – links between cell metabolism and actin remodeling. Journal of Cell Science *134*, jcs248385. 10.1242/jcs.248385.

12. Mosier, J.A., Wu, Y., and Reinhart-King, C.A. (2021). Recent advances in understanding the role of metabolic heterogeneities in cell migration. Fac Rev *10*. 10.12703/r/10-8.

13. Poukkula, M., Cliffe, A., Changede, R., and Rorth, P. (2011). Cell behaviors regulated by guidance cues in collective migration of border cells. J Cell Biol *192*, 513–524. 10.1083/jcb.201010003.

14. Prasad, M., and Montell, D.J. (2007). Cellular and molecular mechanisms of border cell migration analyzed using time-lapse live-cell imaging. Dev Cell *12*, 997–1005. 10.1016/j.devcel.2007.03.021.

15. Boye, E., and Grallert, B. (2020). eIF2α phosphorylation and the regulation of translation. Curr Genet *66*, 293–297. 10.1007/s00294-019-01026-1.

16. Pakos-Zebrucka, K., Koryga, I., Mnich, K., Ljujic, M., Samali, A., and Gorman, A.M. (2016). The integrated stress response. EMBO Rep *17*, 1374–1395. 10.15252/embr.201642195.

17. Donnelly, N., Gorman, A.M., Gupta, S., and Samali, A. (2013). The eIF2α kinases: their structures and functions. Cell. Mol. Life Sci. *70*, 3493–3511. 10.1007/s00018-012-1252-6.

18. Neill, G., and Masson, G.R. (2023). A stay of execution: ATF4 regulation and potential outcomes for the integrated stress response. Front. Mol. Neurosci. *16*, 1112253. 10.3389/fnmol.2023.1112253.

19. Brown, B., Mitra, S., Roach, F.D., Vasudevan, D., and Ryoo, H.D. (2021). The transcription factor Xrp1 is required for PERK-mediated antioxidant gene induction in Drosophila. eLife *10*, e74047. 10.7554/eLife.74047.

20. Hicks, D., Giresh, K., Wrischnik, L.A., and Weiser, D.C. (2023). The PPP1R15 Family of eIF2-alpha Phosphatase Targeting Subunits (GADD34 and CReP). IJMS *24*, 17321. 10.3390/ijms242417321.

21. Malzer, E., Szajewska-Skuta, M., Dalton, L.E., Thomas, S.E., Hu, N., Skaer, H., Lomas, D.A., Crowther, D.C., and Marciniak, S.J. (2013). Coordinate regulation of eIF2α phosphorylation by dPPP1R15 and dGCN2 is required during development. J. Cell Sci, jcs.117614. 10.1242/jcs.117614.

22. Costa-Mattioli, M., and Walter, P. (2020). The integrated stress response: From mechanism to disease. Science *368*, eaat5314. 10.1126/science.aat5314.

23. Chen, Y., Kotian, N., Aranjuez, G., Chen, L., Messer, C.L., Burtscher, A., Sawant, K., Ramel, D., Wang, X., and McDonald, J.A. (2020). Protein phosphatase 1 activity controls a balance between collective and single cell modes of migration. eLife *9*, e52979. 10.7554/eLife.52979.

24. Bertolotti, A. (2018). The split protein phosphatase system. Biochemical Journal *475*, 3707–3723. 10.1042/BCJ20170726.

25. Bennett, D., and Alphey, L. (2002). PP1 binds Sara and negatively regulates Dpp signaling in Drosophila melanogaster. Nat Genet *31*, 419–423. 10.1038/ng938.

26. Hendrickx, A., Beullens, M., Ceulemans, H., Den Abt, T., Van Eynde, A., Nicolaescu, E., Lesage, B., and Bollen, M. (2009). Docking motif-guided mapping of the interactome of protein phosphatase-1. Chem. Biol. *16*, 365–371. 10.1016/j.chembiol.2009.02.012.

27. Sacco, F., Perfetto, L., Castagnoli, L., and Cesareni, G. (2012). The human phosphatase interactome: An intricate family portrait. FEBS Letters *586*, 2732–2739. 10.1016/j.febslet.2012.05.008.

28. Choy, M.S., Yusoff, P., Lee, I.C., Newton, J.C., Goh, C.W., Page, R., Shenolikar, S., and Peti, W. (2015). Structural and Functional Analysis of the GADD34:PP1 eIF2α Phosphatase. Cell Reports *11*, 1885–1891. 10.1016/j.celrep.2015.05.043.

29. Caswell, P.T., and Zech, T. (2018). Actin-Based Cell Protrusion in a 3D Matrix. Trends in Cell Biology *28*, 823–834. 10.1016/j.tcb.2018.06.003.

30. Niewiadomska, P., Godt, D., and Tepass, U. (1999). DE-Cadherin Is Required for Intercellular Motility during Drosophila Oogenesis. Journal of Cell Biology *144*, 533–547. 10.1083/jcb.144.3.533.

31. Wang, H., Qiu, Z., Xu, Z., Chen, S.J., Luo, J., Wang, X., and Chen, J. (2018). aPKC is a key polarity determinant in coordinating the function of three distinct cell polarities during collective migration. Development *145*, dev158444. 10.1242/dev.158444.

32. Sonenberg, N., and Hinnebusch, A.G. (2009). Regulation of Translation Initiation in Eukaryotes: Mechanisms and Biological Targets. Cell *136*, 731–745. 10.1016/j.cell.2009.01.042.

33. Malzer, E., Daly, M.-L., Moloney, A., Sendall, T.J., Thomas, S.E., Ryder, E., Ryoo, H.D., Crowther, D.C., Lomas, D.A., and Marciniak, S.J. (2010). Impaired tissue growth is mediated by checkpoint kinase 1 (CHK1) in the integrated stress response. Journal of Cell Science *123*, 2892–2900. 10.1242/jcs.070078.

34. Bjordal, M., Arquier, N., Kniazeff, J., Pin, J.P., and Léopold, P. (2014). Sensing of Amino Acids in a Dopaminergic Circuitry Promotes Rejection of an Incomplete Diet in Drosophila. Cell *156*, 510–521. 10.1016/j.cell.2013.12.024.

35. Hetz, C., Zhang, K., and Kaufman, R.J. (2020). Mechanisms, regulation and functions of the unfolded protein response. Nat Rev Mol Cell Biol *21*, 421–438. 10.1038/s41580-020-0250-z.

36. Katow, H., Vasudevan, D., and Ryoo, H.D. (2022). Drosophila Unfolded Protein Response (UPR) Assays In Vitro and In Vivo. In The Unfolded Protein Response Methods in Molecular Biology., R. Pérez-Torrado, ed. (Springer US), pp. 261–277. 10.1007/978-1-0716-1732-8_17.

37. Dubois, C., Prevarskaya, N., and Vanden Abeele, F. (2016). The calcium-signaling toolkit: Updates needed. Biochimica et Biophysica Acta (BBA) - Molecular Cell Research *1863*, 1337–1343. 10.1016/j.bbamcr.2015.11.033.

38. Guo, X., Luo, J., Wang, H., and Chen, J. (2019). SERCA regulates collective cell migration by maintaining cytoplasmic Ca2+ homeostasis. Journal of Genetics and Genomics *46*, 451–454. 10.1016/j.jgg.2019.09.001.

39. Liu, J., Xu, Y., Stoleru, D., and Salic, A. (2012). Imaging protein synthesis in cells and tissues with an alkyne analog of puromycin. Proc. Natl. Acad. Sci. U.S.A. *109*, 413–418. 10.1073/pnas.1111561108.

40. Kiparaki, M., Khan, C., Folgado-Marco, V., Chuen, J., Moulos, P., and Baker, N.E. (2022). The transcription factor Xrp1 orchestrates both reduced translation and cell competition upon defective ribosome assembly or function. eLife *11*, e71705. 10.7554/eLife.71705.

41. Grmai, L., Michaca, M., Lackner, E., and Vasudevan, D. (2023). Integrated Stress Response signaling acts as a metabolic sensor in fat tissues to regulate oocyte maturation and ovulation. bioRxiv. 10.1101/2023.02.27.530289.

42. Vasudevan, D., Katow, H., Huang, H.-W., Tang, G., and Ryoo, H.D. (2022). A protein-trap allele reveals roles for *Drosophila* ATF4 in photoreceptor degeneration, oogenesis and wing development. Disease Models & Mechanisms *15*, dmm049119. 10.1242/dmm.049119.

43. Lee, C.-H., Kiparaki, M., Blanco, J., Folgado, V., Ji, Z., Kumar, A., Rimesso, G., and Baker, N.E. (2018). A Regulatory Response to Ribosomal Protein Mutations Controls Translation, Growth, and Cell Competition. Developmental Cell *46*, 456-469.e4. 10.1016/j.devcel.2018.07.003.

44. Vasudevan, D., and Ryoo, H.D. (2016). Detection of Cell Death in Drosophila Tissues. In Programmed Cell Death Methods in Molecular Biology., H. Puthalakath and C. J. Hawkins, eds. (Springer New York), pp. 131–144. 10.1007/978-1-4939-3581-9_11.

45. Tabas, I., and Ron, D. (2011). Integrating the mechanisms of apoptosis induced by endoplasmic reticulum stress. Nat Cell Biol *13*, 184–190. 10.1038/ncb0311-184.

46. Borensztejn, A., Boissoneau, E., Fernandez, G., Agnès, F., and Pret, A.-M. (2013). JAK/STAT autocontrol of ligand-producing cell number through apoptosis. Development *140*, 195–204. 10.1242/dev.079046.

47. Hay, B.A., Wolff, T., and Rubin, G.M. (1994). Expression of baculovirus P35 prevents cell death in Drosophila. Development *120*, 2121–2129. 10.1242/dev.120.8.2121.

48. Shacham, T., Patel, C., and Lederkremer, G.Z. (2021). PERK Pathway and Neurodegenerative Disease: To Inhibit or to Activate? Biomolecules *11*, 354. 10.3390/biom11030354.

49. Bobrovnikova-Marjon, E., Hatzivassiliou, G., Grigoriadou, C., Romero, M., Cavener, D.R., Thompson, C.B., and Diehl, J.A. (2008). PERK-dependent regulation of lipogenesis during mouse mammary gland development and adipocyte differentiation. Proc. Natl. Acad. Sci. U.S.A. *105*, 16314–16319. 10.1073/pnas.0808517105.

50. Chen, C.-W., Guan, B.-J., Alzahrani, M.R., Gao, Z., Gao, L., Bracey, S., Wu, J., Mbow, C.A., Jobava, R., Haataja, L., et al. (2022). Adaptation to chronic ER stress enforces pancreatic β-cell plasticity. Nat Commun *13*, 4621. 10.1038/s41467-022-32425-7.

51. Malzer, E., Dominicus, C.S., Chambers, J.E., Dickens, J.A., Mookerjee, S., and Marciniak, S.J. (2018). The integrated stress response regulates BMP signalling through effects on translation. BMC Biol *16*, 34. 10.1186/s12915-018-0503-x.

52. Harding, H.P., Zhang, Y., Scheuner, D., Chen, J.-J., Kaufman, R.J., and Ron, D. (2009). Ppp1r15 gene knockout reveals an essential role for translation initiation factor 2 alpha

(eIF2alpha) dephosphorylation in mammalian development. Proc. Natl. Acad. Sci. U.S.A. *106*, 1832–1837. 10.1073/pnas.0809632106.

53. Shayya, H.J., Kahiapo, J.K., Duffié, R., Lehmann, K.S., Bashkirova, L., Monahan, K., Dalton, R.P., Gao, J., Jiao, S., Schieren, I., et al. (2022). ER stress transforms random olfactory receptor choice into axon targeting precision. Cell *185*, 3896-3912.e22. 10.1016/j.cell.2022.08.025.

54. Limia, C., Sauzay, C., Urra, H., Hetz, C., Chevet, E., and Avril, T. (2019). Emerging Roles of the Endoplasmic Reticulum Associated Unfolded Protein Response in Cancer Cell Migration and Invasion. Cancers *11*, 631. 10.3390/cancers11050631.

55. Tanaka, C., Ito, S., Nishio, N., Kodera, Y., Sakurai, H., Suzuki, H., Nakao, A., and Isobe, K.-I. (2010). GADD34 suppresses wound healing by upregulating expression of myosin IIA. Transgenic Res *19*, 637–645. 10.1007/s11248-009-9347-z.

56. Feng, Y., Sokol, E.S., Del Vecchio, C.A., Sanduja, S., Claessen, J.H.L., Proia, T.A., Jin, D.X., Reinhardt, F., Ploegh, H.L., Wang, Q., et al. (2014). Epithelial-to-Mesenchymal Transition Activates PERK–eIF2α and Sensitizes Cells to Endoplasmic Reticulum Stress. Cancer Discovery *4*, 702–715. 10.1158/2159-8290.CD-13-0945.

57. Miao, G., Godt, D., and Montell, D.J. (2020). Integration of Migratory Cells into a New Site In Vivo Requires Channel-Independent Functions of Innexins on Microtubules. Developmental Cell *54*, 501-515.e9. 10.1016/j.devcel.2020.06.024.

58. Saarikangas, J., Zhao, H., and Lappalainen, P. (2010). Regulation of the Actin Cytoskeleton-Plasma Membrane Interplay by Phosphoinositides. Physiological Reviews *90*, 259–289. 10.1152/physrev.00036.2009.

59. Han, J., and Kaufman, R.J. (2016). The role of ER stress in lipid metabolism and lipotoxicity. Journal of Lipid Research *57*, 1329–1338. 10.1194/jlr.R067595.

60. Radanović, T., and Ernst, R. (2021). The Unfolded Protein Response as a Guardian of the Secretory Pathway. Cells *10*, 2965. 10.3390/cells10112965.

61. Malhotra, J.D., and Kaufman, R.J. (2011). ER Stress and Its Functional Link to Mitochondria: Role in Cell Survival and Death. Cold Spring Harbor Perspectives in Biology *3*, a004424–a004424. 10.1101/cshperspect.a004424.

62. Geisbrecht, E.R., and Montell, D.J. (2004). A Role for Drosophila IAP1-Mediated Caspase Inhibition in Rac-Dependent Cell Migration. Cell *118*, 111–125. 10.1016/j.cell.2004.06.020.

63. Demay, Y., Perochon, J., Szuplewski, S., Mignotte, B., and Gaumer, S. (2014). The PERK pathway independently triggers apoptosis and a Rac1/Slpr/JNK/Dilp8 signaling favoring tissue homeostasis in a chronic ER stress Drosophila model. Cell Death Dis *5*, e1452–e1452. 10.1038/cddis.2014.403.

64. Parlani, M., Jorgez, C., and Friedl, P. (2023). Plasticity of cancer invasion and energy metabolism. Trends in Cell Biology *33*, 388–402. 10.1016/j.tcb.2022.09.009.

65. Sarov, M., Barz, C., Jambor, H., Hein, M.Y., Schmied, C., Suchold, D., Stender, B., Janosch, S., Kj, V.V., Krishnan, R., et al. (2016). A genome-wide resource for the analysis of protein localisation in Drosophila. eLife *5*, e12068. 10.7554/eLife.12068.

66. Dai, W., and Montell, D.J. (2016). Live Imaging of Border Cell Migration in Drosophila. In Chemotaxis Methods in Molecular Biology., T. Jin and D. Hereld, eds. (Springer New York), pp. 153–168. 10.1007/978-1-4939-3480-5_12.

67. Wilcockson, S.G., and Ashe, H.L. (2021). Live imaging of the Drosophila ovarian germline stem cell niche. STAR Protocols *2*, 100371. 10.1016/j.xpro.2021.100371.

68. Schindelin, J., Arganda-Carreras, I., Frise, E., Kaynig, V., Longair, M., Pietzsch, T., Preibisch, S., Rueden, C., Saalfeld, S., Schmid, B., et al. (2012). Fiji: an open-source platform for biological-image analysis. Nat Methods *9*, 676–682. 10.1038/nmeth.2019.

69. Sawant, K., Chen, Y., Kotian, N., Preuss, K.M., and McDonald, J.A. (2018). Rap1 GTPase promotes coordinated collective cell migration in vivo. Mol Biol Cell *29*, 2656–2673. 10.1091/mbc.E17-12-0752.

70. Kluyver, T., Ragan-Kelley, B., Pérez, F., Bussonnier, M., Frederic, J., Hamrick, J., Grout, J., Corlay, S., Ivanov, P., Abdalla, S., et al. (2016). Jupyter Notebooks—a publishing format for reproducible computational workflows. IOS Press. 10.3233/978-1-61499-649-1-87.

71. Van Rossum, G., and Drake, F.L. (2009). Python 3 Reference Manual (CreateSpace).

72. Waskom, M. (2021). seaborn: statistical data visualization. JOSS *6*, 3021. 10.21105/joss.03021.

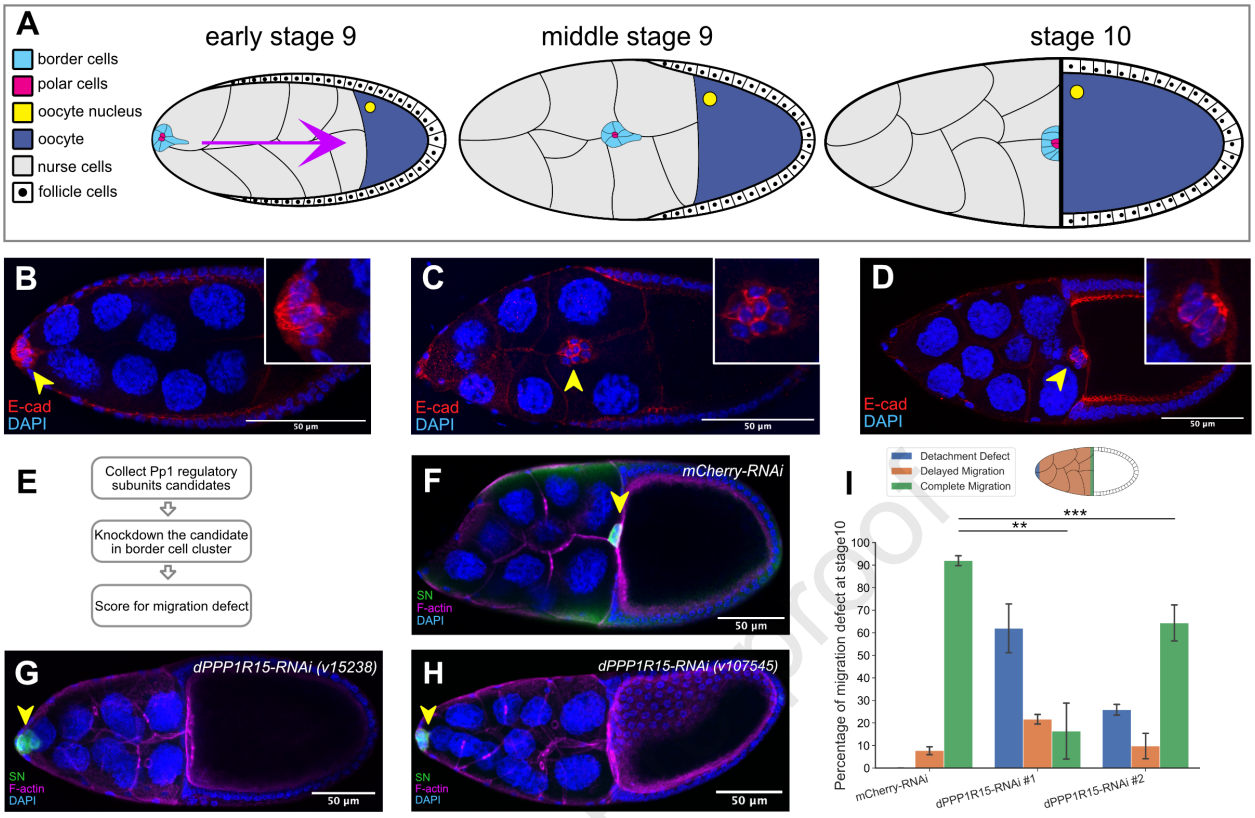

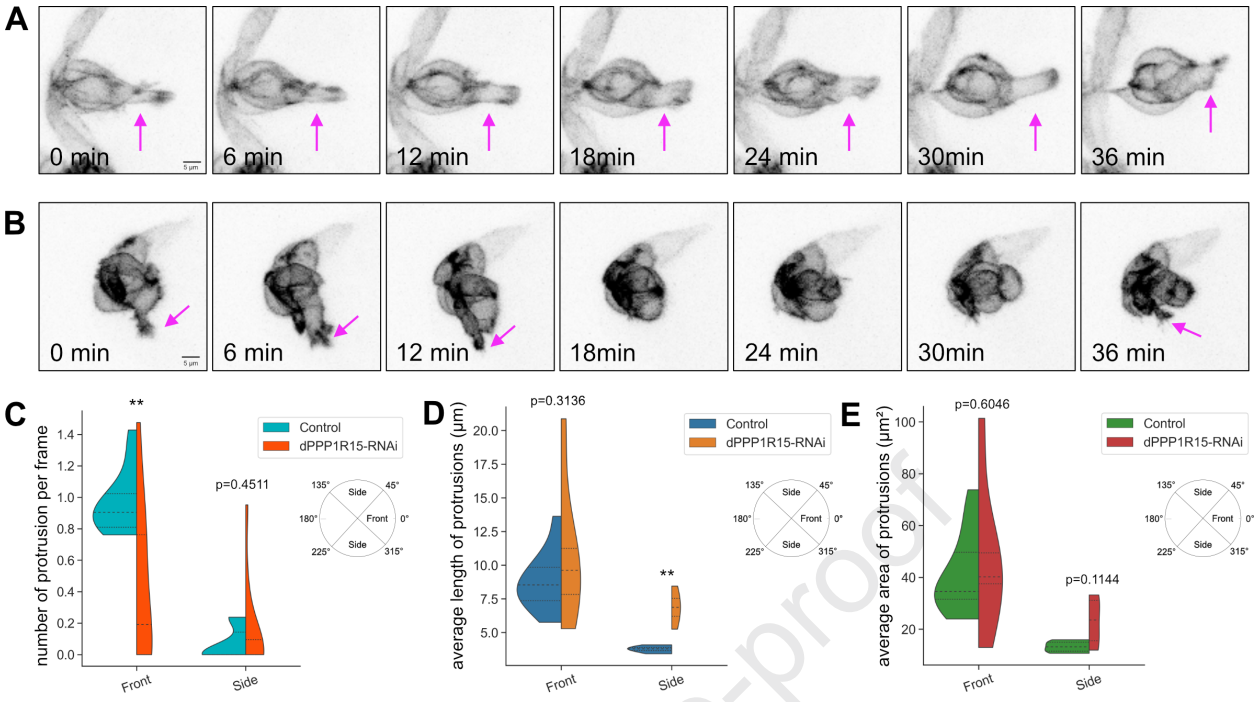

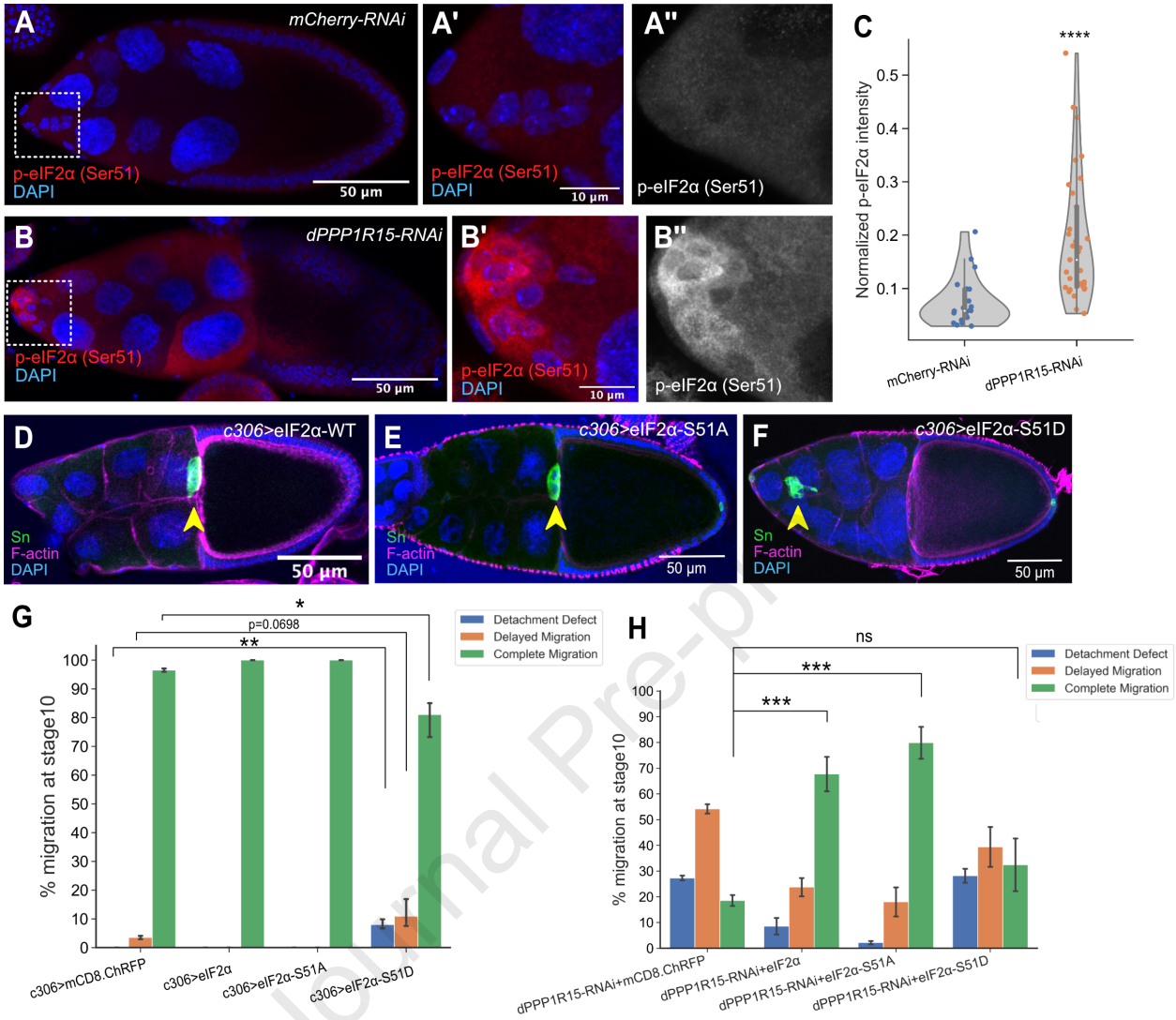

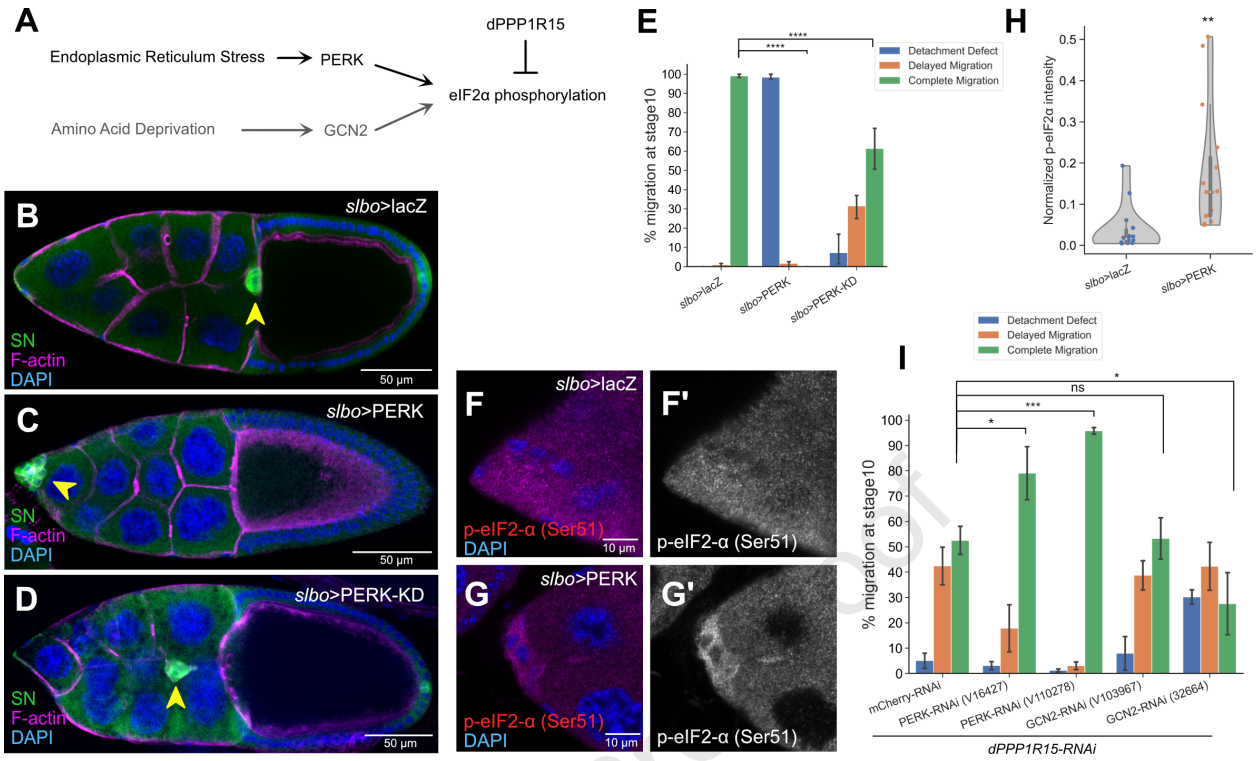

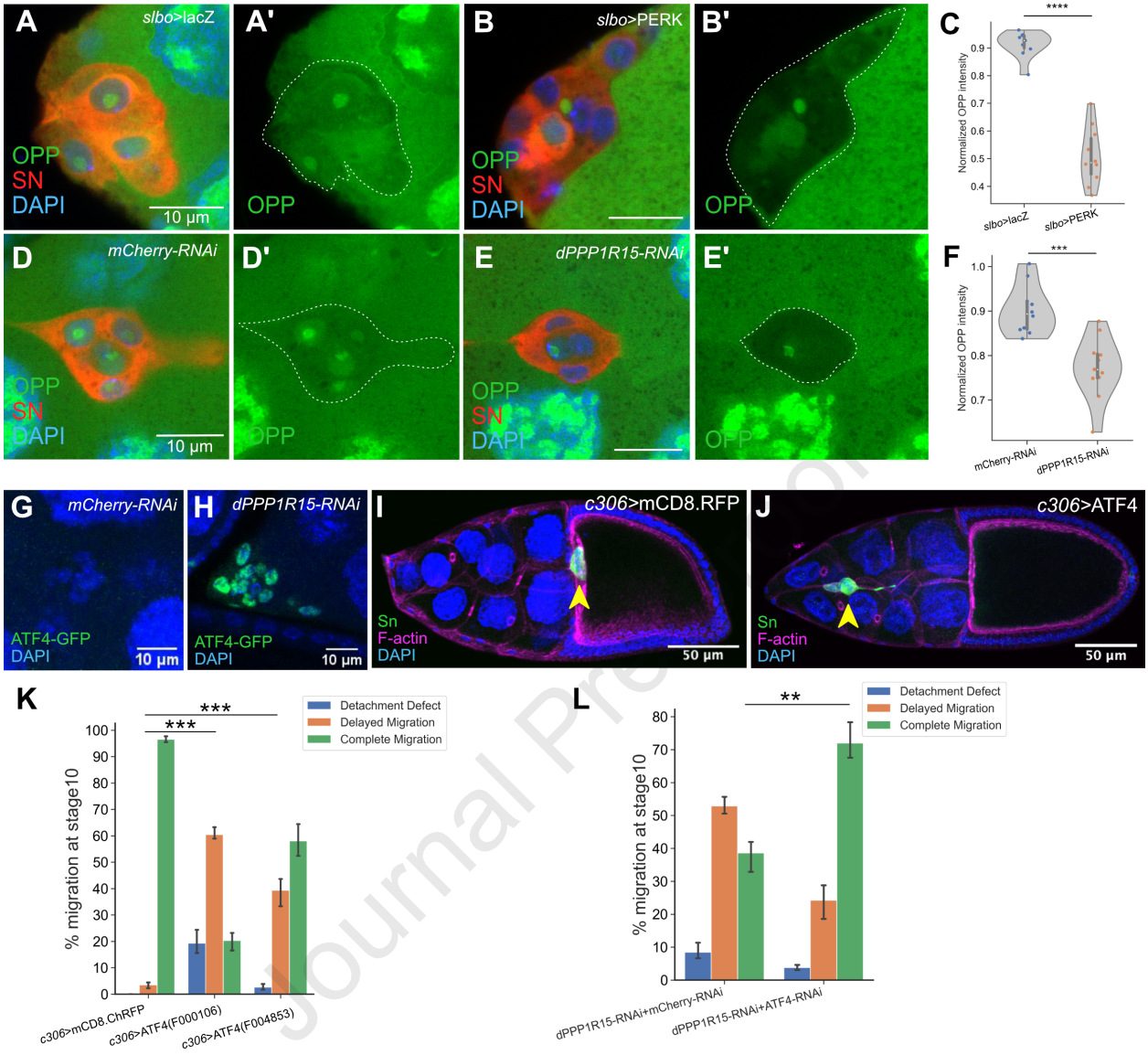
A
slbo>lacZ
OPP
SN
DAPI
10 μm
A'
OPP
B
slbo>PERK
OPP
SN
DAPI
B'
OPP
C
****
Normalized OPP intensity
0.9
0.8
0.7
0.6
0.5
0.4
slbo>lacZ
slbo>PERK
D
mCherry-RNAi
OPP
SN
DAPI
10 μm
D'
OPP
E
dPPP1R15-RNAi
OPP
SN
DAPI
E'
OPP
F
***
Normalized OPP intensity
1.0
0.9
0.8
0.7
mCherry-RNAi
dPPP1R15-RNAi
G
mCherry-RNAi
ATF4-GFP
DAPI
10 μm
H
dPPP1R15-RNAi
ATF4-GFP
DAPI
10 μm
I
c306>mCD8.RFP
Sn
F-actin
DAPI
50 μm
J
c306>ATF4
Sn
F-actin
DAPI
50 μm
K
***
***
Detachment Defect
Delayed Migration
Complete Migration
% migration at stage10
100
90
80
70
60
50
40
30
20
10
0
c306>mCD8.ChRFP
c306>ATF4(F000106)
c306>ATF4(F004853)
L
**
Detachment Defect
Delayed Migration
Complete Migration
% migration at stage10
80
70
60
50
40
30
20
10
0
dPPP1R15-RNAi+mCherry-RNAi
dPPP1R15-RNAi+ATF4-RNAi

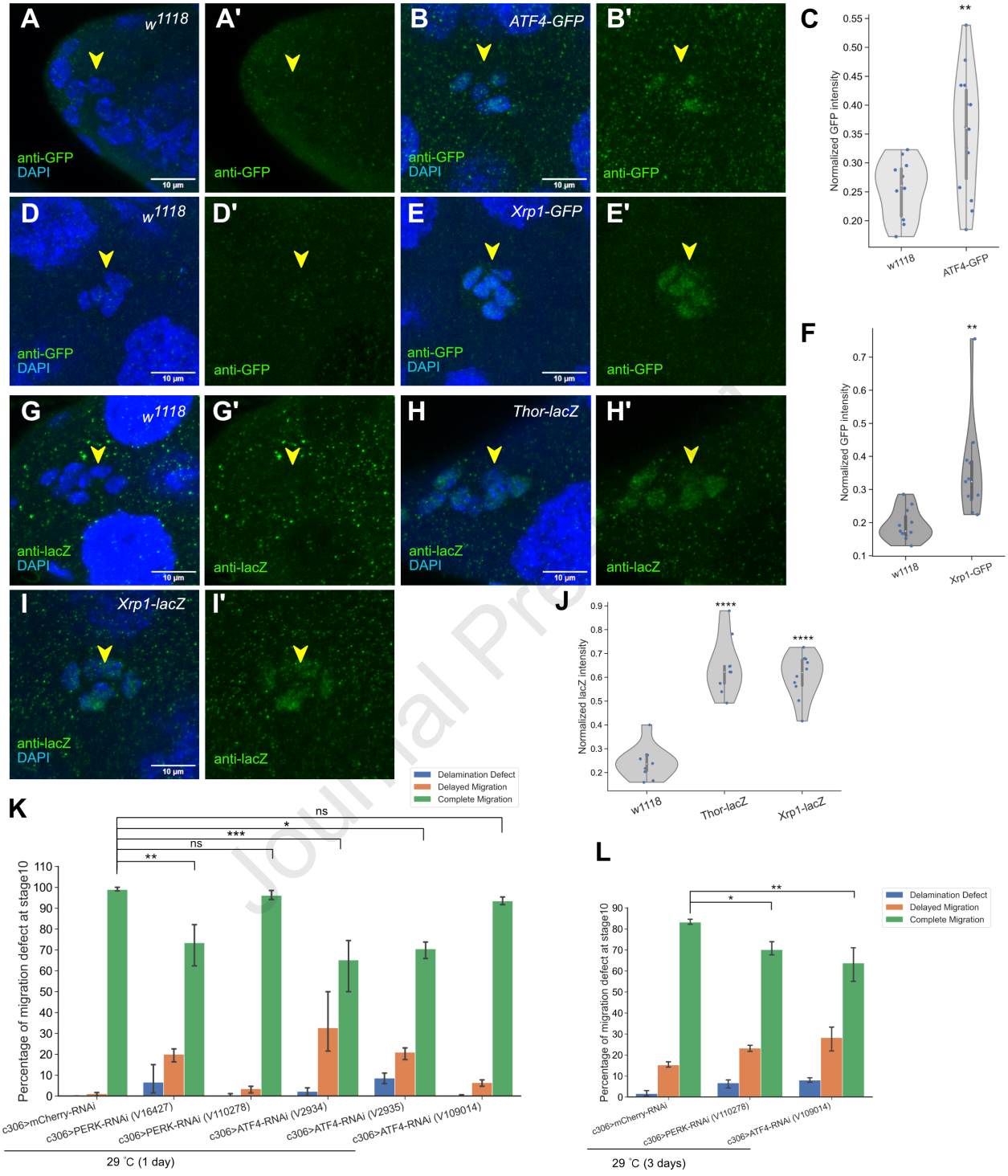
A
w1118
anti-GFP
DAPI
10 μm
A'
anti-GFP
B
ATF4-GFP
anti-GFP
DAPI
10 μm
B'
anti-GFP
C
**
Normalized GFP intensity
0.55
0.50
0.45
0.40
0.35
0.30
0.25
0.20
w1118
ATF4-GFP
D
w1118
anti-GFP
DAPI
10 μm
D'
anti-GFP
E
Xrp1-GFP
anti-GFP
DAPI
10 μm
E'
anti-GFP
F
**
Normalized GFP intensity
0.7
0.6
0.5
0.4
0.3
0.2
0.1
w1118
Xrp1-GFP
G
w1118
anti-lacZ
DAPI
10 μm
G'
anti-lacZ
H
Thor-lacZ
anti-lacZ
DAPI
10 μm
H'
anti-lacZ
I
Xrp1-lacZ
anti-lacZ
DAPI
10 μm
I'
anti-lacZ
J
****
****
Normalized lacZ intensity
0.9
0.8
0.7
0.6
0.5
0.4
0.3
0.2
w1118
Thor-lacZ
Xrp1-lacZ
Delamination Defect
Delayed Migration
Complete Migration
K
ns
*
***
ns
**
Percentage of migration defect at stage10
110
100
90
80
70
60
50
40
30
20
10
0
c306>mCherry-RNAi
c306>PERK-RNAi (V16427)
c306>PERK-RNAi (V110278)
c306>ATF4-RNAi (V2934)
c306>ATF4-RNAi (V2935)
c306>ATF4-RNAi (V109014)
29 ℃ (1 day)
L
**
*
Percentage of migration defect at stage10
90
80
70
60
50
40
30
20
10
0
c306>mCherry-RNAi
c306>PERK-RNAi (V110278)
c306>ATF4-RNAi (V109014)
29 ℃ (3 days)
Delamination Defect
Delayed Migration
Complete Migration

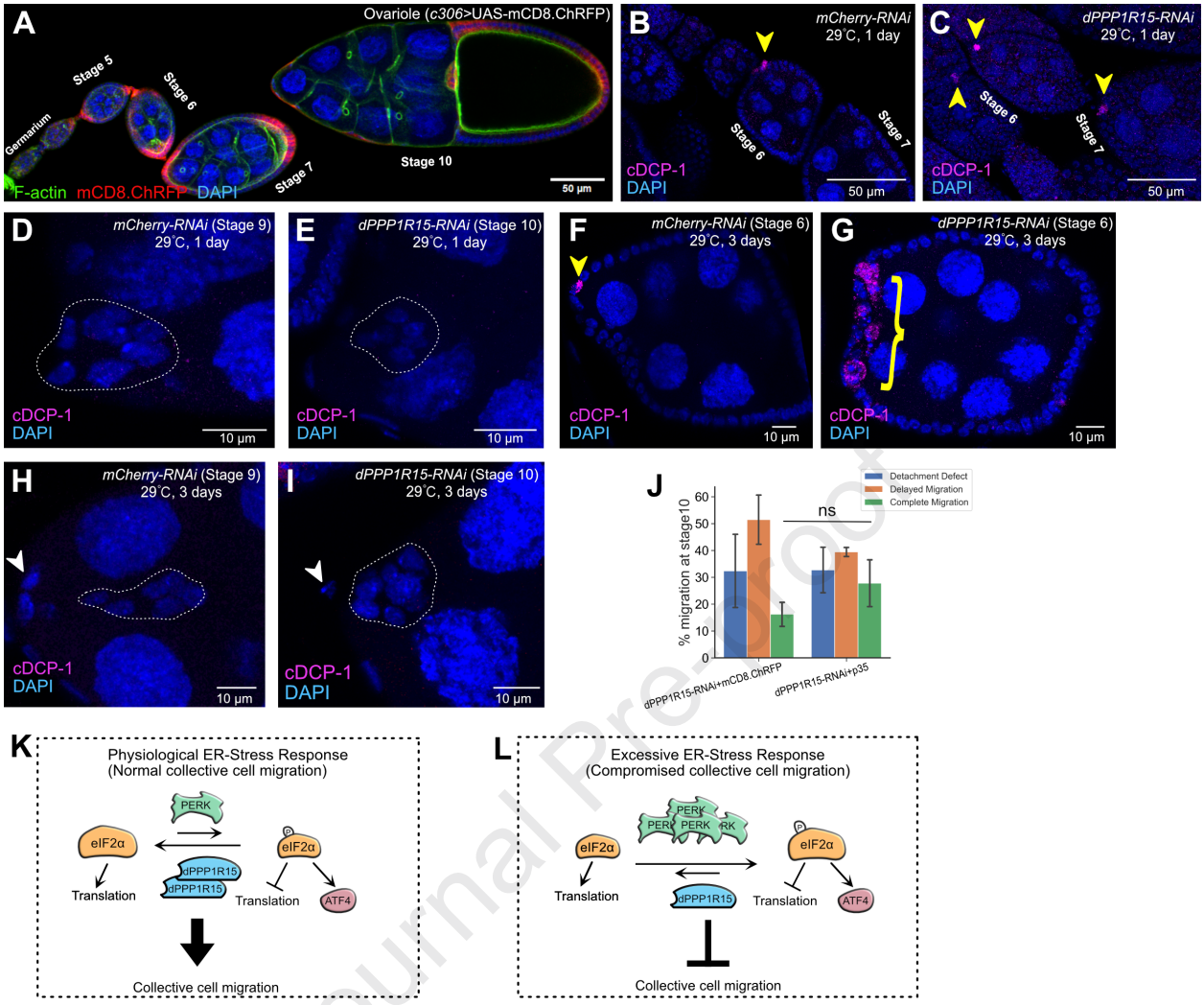

eTOC Blurb

Precise control of endoplasmic reticulum (ER) stress ensures cell health. Chen and McDonald show that normal migrating border cells exhibit physiological ER stress that is restrained by dPPP1R15. This regulation prevents excessive activation of the PERK-p-eIF2α-ATF4 ER stress response pathway, ensuring effective collective border cell migration.

Highlights

- dPPP1R15 disruption impairs border cell collective delamination and migration
- dPPP1R15 is essential for tightly regulated front-directed protrusions
- Normal collectively migrating border cells exhibit physiological ER stress
- dPPP1R15 limits PERK-eIF2α-ATF4 ER stress response for border cell migration

KEY RESOURCES TABLE

REAGENT or RESOURCE	SOURCE	IDENTIFIER
Antibodies		
Monoclonal rat anti-E-cadherin (1:10 dilution)	Developmental Studies Hybridoma Bank	Cat#DCAD2
Monoclonal mouse anti-Singed (Fascin) (1:10 dilution)	Developmental Studies Hybridoma Bank	Cat#7G10
Monoclonal mouse anti-lacZ (1:10 dilution)	Developmental Studies Hybridoma Bank	Cat#40-1a
Monoclonal mouse anti-Dlg (1:10 dilution)	Developmental Studies Hybridoma Bank	Cat#4F3
Rabbit anti-aPKC (1:200 dilution)	Santa Cruz Biotechnology, Inc.	Cat#H1904
Phospho-eIF2α (Ser51) (119A11) Rabbit (1:50 dilution)	Cell Signaling Technology, Inc.	Cat# 3597
Anti-EIF2S1 antibody (1:100 dilution)	Abcam	Cat# ab26197
Cleaved Caspase-3 (Asp175) Antibody (1:50 dilution)	Cell Signaling Technology, Inc.	Cat#9661
Polyclonal rabbit anti-GFP (1:2000 dilution)	Thermo Fisher Scientific	Cat#A11122
Chemicals, peptides, and recombinant proteins		
IgG1 Cross-Adsorbed Goat anti-Mouse, Alexa Fluor™ 568 (1:400 dilution)	Thermo Fisher Scientific	Cat#A21124
IgG1 Cross-Adsorbed Goat anti-Mouse, Alexa Fluor™ 488 (1:400 dilution)	Thermo Fisher Scientific	Cat#A21121
Goat anti-Mouse IgG (H+L) Highly Cross-Adsorbed Secondary Antibody, Alexa Fluor™ 647	Thermo Fisher Scientific	Cat#A21236
Goat anti-Rabbit IgG (H+L) Highly Cross-Adsorbed Secondary Antibody, Alexa Fluor™ 568	Thermo Fisher Scientific	Cat#A11036
Phalloidin-Atto 647N (1:400)	Millipore Sigma	Cat#65906
Halocarbon oil 27	Millipore Sigma	Cat#9002-83-9
Insulin, Recombinant Human	Millipore Sigma	Cat#11061-68-0
Fibrinogen, bovine plasma	Millipore Sigma	Cat#341573
Thrombin protease	Millipore Sigma	Cat# GE27-0846-01
4',6-Diamidino-2-phenylindole (DAPI)	Millipore Sigma	Cat#D9542
Schneider's Drosophila Medium	Gibco	Cat#21720
Paraformaldehyde, 16% solution	Electron Microscopy Sciences	Cat#15710
Phusion Site-Directed Mutagenesis Kit	Thermo Fisher Scientific	Cat#F541
Click-iT™ Plus EdU Alexa Fluor™ 488 Imaging Kit	Thermo Fisher Scientific	Cat#C10637
dPPP1R15-GFP fosmid reporter DNA: FlyFos030422(pRedFlp-Hgr)(Gadd34[28715]::S000169_fly_pretag)::2XTY1-SGFP-V5-preTEV-BLRP-3XFLAGdFRT	Sarov et al.[65]; https://transgeneome.mpi-cbg.de/transgeneomics/	Cat#Clone_6581804 864395902 E11
dPPP1R15 cDNA	Drosophila Genomics Resource Center	Cat#DGRC_7249
eIF2α cDNA	Drosophila Genomics Resource Center	Cat#DGRC_1613078
pUASg-HA-attB	Drosophila Genomics Resource Center	Cat#DGRC_1423
Experimental models: Organisms/strains		
D. melanogaster: w[1118]	Bloomington Drosophila Stock Center	BDSC:3605
D. melanogaster: c306-GAL4	Bloomington Drosophila Stock Center	BDSC:3743
D. melanogaster: c306-GAL4 tsGAL80	Created in our lab	N/A
D. melanogaster: slbo-Gal4	From Denise Montell	N/A
D. melanogaster: UAS-PLCδ-PH-GFP	Bloomington Drosophila Stock Center	BDSC:39693
D. melanogaster: UAS-Pp1-87B.HA	Bloomington Drosophila Stock Center	BDSC:24098
D. melanogaster: UAS-Pp1-13C.HA	Bloomington Drosophila Stock Center	BDSC:23701
D. melanogaster: UAS-Pp1alpha-96A.HA	Bloomington Drosophila Stock Center	BDSC:23700
D. melanogaster: UAS-hPPP1CC.HA	Bloomington Drosophila Stock Center	BDSC:64395
D. melanogaster: UAS-mCherry RNAi	Bloomington Drosophila Stock Center	BDSC:35785
D. melanogaster: UAS-Flw.HA	The Zurich ORFeome Project,FlyORF	Line F001200
D. melanogaster: w[*]; P{w[+mC]=UAS-p35.H}BH1	Bloomington Drosophila Stock Center	BDSC:5072

D. melanogaster: y[1] w[67c23]; Mi{PT-GFSTF.1}crc[MI02300-GFSTF.1]	Bloomington Drosophila Stock Center	BDSC:59608
D. melanogaster: y[1] w[*]; P{y[+t7.7] w[+mC]=Xrp1-GFP.FPTB}attP40	Bloomington Drosophila Stock Center	BDSC:83391
D. melanogaster: ry[506] P{ry[+t7.2]=PZ}Xrp1[02515]/TM3, ry[RK] Sb[1] Ser[1]	Bloomington Drosophila Stock Center	BDSC:11569
D. melanogaster: y[1] w[*]; P{w[+mC]=lacW}Thor[k13517]	Bloomington Drosophila Stock Center	BDSC:9558
D. melanogaster: w[*]; P{w[+mC]=UAS-Xbp1.EGFP.LG}2/CyO	Bloomington Drosophila Stock Center	BDSC:39720
D. melanogaster: UAS-mCD8.ChRFP	Bloomington Drosophila Stock Center	BDSC:27392
D. melanogaster: UAS-dPPP1R15 RNAi	Vienna Drosophila Resource Center	VDRC:15328
D. melanogaster: UAS-dPPP1R15 RNAi	Vienna Drosophila Resource Center	VDRC:107545
D. melanogaster: UAS-PERK	Bloomington Drosophila Stock Center	BDSC:76248
D. melanogaster: UAS-PERK-KD (kinase dead form)	Bloomington Drosophila Stock Center	BDSC:76249
D. melanogaster: UAS-PERK-RNAi	Vienna Drosophila Resource Center	VDRC:16427
D. melanogaster: UAS-PERK-RNAi	Bloomington Drosophila Stock Center	VDRC:110278
D. melanogaster: UAS-ATF4-RNAi	Bloomington Drosophila Stock Center	BDSC:25985
D. melanogaster: UAS-ATF4-RNAi	Vienna Drosophila Resource Center	VDRC:2534
D. melanogaster: UAS-ATF4-RNAi	Vienna Drosophila Resource Center	VDRC:2535
D. melanogaster: UAS-ATF4-RNAi	Vienna Drosophila Resource Center	VDRC:109014
D. melanogaster: UAS-SERCA-RNAi	Vienna Drosophila Resource Center	VDRC:4474
D. melanogaster: UAS-ATF4	Zurich ORFeome Project	FlyORF:F000106
D. melanogaster: UAS-ATF4	Zurich ORFeome Project	FlyORF:F004853
D. melanogaster: UAS-GCN2-RNAi	Vienna Drosophila Resource Center	VDRC:103967
D. melanogaster: UAS-GCN2-RNAi	Vienna Drosophila Resource Center	VDRC:32664
D. melanogaster: dPPP1R15-GFP fosmid reporter	This paper	N/A
D. melanogaster: UAS-dPPP1R15	This paper	N/A
D. melanogaster: UAS-dPPP1R15-V249E	This paper	N/A
D. melanogaster: UAS-dPPP1R15-V257A, H258A	This paper	N/A
D. melanogaster: UAS-PPP1R15B	This paper	N/A
D. melanogaster: UAS-eIF2α	This paper	N/A
D. melanogaster: UAS-eIF2α-S51A	This paper	N/A
D. melanogaster: UAS-eIF2α-S51D	This paper	N/A
Software and algorithms		
ImageJ2 (FIJI)	Schindelin et al.[68]	N/A
Affinity Designer 1.7.1	https://affinity.serif.com/	N/A
Zeiss AxioVision 4.8	Zeiss	N/A
Zeiss ZEN 3.0	Zeiss	N/A
Jupyter Notebook	Kluyver et al.[70]	N/A
Python 3.7	Van Rossum and Drake[71]	N/A
Seaborn	Waskom[72]	N/A
Graphpad Prism 7, Prism 8	www.graphpad.com	N/A
Other		
Zeiss Axio Imager Z1 with Apotome2 microscope	Carl Zeiss	N/A
Zeiss LSM800 Confocal	Carl Zeiss	N/A
Zeiss LSM880 Confocal	Carl Zeiss	N/A